Numerical comparisons of traffic flow models

Niyitegeka, C.

Award date:
2015

Numerical Comparisons of Traffic Flow Models

Colette Niyitegeka

Supervised by

Prof. Dr. Axel Klar (TU Kaiserslautern, Germany)

and

Dr. J.H.M. ten Thije Boonkkamp (TU Eindhoven, Netherlands)

Thesis submitted to the Departments of Mathematics, TU Kaiserslautern and TU Eindhoven in partial fulfillment of the requirements for the award of Master of Science degree in Mathematics

Abstract

In the past several years, the fast growing number of vehicles on long crowded roads motivated an intense scientific research activity in the field of traffic flow modeling. In this thesis we present and discuss some of the macroscopic models of vehicular traffic flow; the first order LWR model and second order Aw-Rascle model are both solved analytically and numerically. We study the Riemann problems of these models and present some numerical similarities as well as differences between the two models. We perform several numerical experiments in order to verify some qualitative traffic flow behaviour for various traffic parameters in our models. All numerical simulations presented in this thesis are obtained by implementing the first order Godunov-type approximation together with the CFL condition for the stability test of the solutions. In our numerical tests we will show that the Aw-Rascle model predicts instabilities for very light traffic, even with few slow drivers that could not be predicted by the LWR model.

Contents

Chapter 1

Introduction

1.1 Motivation and Definition of the Problem

Traffic networks consisting of highways, streets, and other kinds of roadways are very important in management of traffic situations; they provide convenient and economical conveyance of passengers and goods. Nowadays, in my home country, the fast growing number of vehicles on urban streets and roadways together with related economical and social implications, such as, prevention of car crashes, pollution and energy control, has motivated me to go into this research activity in the field of traffic flow modeling. In my country there are always traffic jams but my experience in Europe, especially here in Germany, is different as far as traffic flow is concerned. I have realised that the flow of traffic is very smooth in this area of the world. As someone who believes in helping my nation, I know doing my research about traffic flow models will be very beneficial to my home country in the future. This motivated me to go into this research since it will open my understanding of traffic situations and how to mathematically model the problem. I believe at the end of this research I will be equipped with the needed mathematical tools to go into further studies and practise in the field of traffic flow management.

Traffic flow can be defined as the study of the movement of individual drivers and vehicles between two points: origin/destination, and the interactions they make with one another. Unfortunately, studying traffic flow is difficult because driver behavior is something that cannot be predicted with one-hundred percent certainty. Fortunately, drivers tend to behave within a reasonably consistent range and, thus, traffic streams tend to have some reasonable consistency and can be roughly represented mathematically. To better represent traffic flow, relationships have been established between the three main characteristics: flow, density and mean velocity, which are, in this thesis, represented by q, ρ, and v, respectively. Vehicular traffic flow can be viewed as an engineering and also a challenging mathematical problem [13]. However, both applied mathematicians and engineers are involved in this field: mathematicians have been able to develop suitable methods which describe the evolution in time and space of the flow conditions, such as, car density and velocity. In addition, mathematical research also consists in solving mathematical problems generated by the application of models to real traffic flow conditions. The output may hopefully be useful for engineers involved in traffic flow control and optimization [14].

There have been developed three different types of models in mathematical modeling of traffic flows: microscopic, kinetic and macroscopic models, see, e.g., [11, 12, 13, 14]. *Microscopic* modeling corresponds to model the dynamics of each single vehicle under the action

of the surrounding vehicles by ordinary differential equations based on Newton's law, in other words all vehicles are individually identified. Position and velocity of each vehicle define the state of the system as dependent variables of the time variable. This is also called car following models [12, 14]. On the other hand, *macroscopic* ones model traffic flows, such as flow rate q, traffic density ρ and travel speed v, as a continuum [15], i.e., the state is described by locally averaged quantities, i.e. $q,\ \rho,\ v$ are considered as dependent variables of time and space. The basic relationship between these variables is $q = \rho v$. Lastly, the *kinetic* modeling as well requires in principle a large number of particles in the system but, unlike the macroscopic approach, it is based on a microscopic modeling of their mutual interactions [11]. For example, let us measure the velocity of a car moving along a highway. The most common way to do this is to record the velocity $v_i = dx_i/dt$ of each car. With N cars there are N different velocities, $v_i(t),\ i = 1, \cdot, \cdot, \cdot, N$, each depending on time. This describes the microscopic model of traffic flows. If the number of cars N is large, this model becomes more complex since it is difficult to keep track of each car. On the other hand, instead of measuring the velocity of each individual car, we associate to each point x in space at each time t a velocity field, $v(x, t)$. This would be the velocity measured at position x at time t. This defines the macroscopic model.

Among the above three types of model, macroscopic models are more suitable for modeling traffic flow in complex networks since less supporting data and computation are needed. In this thesis some of macroscopic traffic flow models are studied both analytically and numerically; we propose the first-order and second-order models (here the order refers to the number of equations that form the model). Traffic flows are classified according to traffic conditions, roadway conditions and traffic network structure. We say that traffic flows are in *equilibrium* when their travel speed is uniquely determined as a function of the traffic density, otherwise they are in *non-equilibrium*. The simplest situation in traffic flow theory is the *homogeneous* equilibrium traffic flow [12], that is, a uniform flow of vehicles not depending on space and time variables; here the state of the traffic flow only depends on the vehicles density. Traffic flows are considered *inhomogeneous* when the roadway has different parameters at different locations.

In this thesis we focus on equilibrium traffic flows. The most elementary continuum traffic flow model was the first order model developed by Lighthill, Whitham (1955) and Richards (1956) [18], based on the assumption of mass density conservation, that is, the number of vehicles between any two points if there are no entrances or exits is conserved. This model is based on the idea that the classical Euler and Navier-Stokes equations of fluid dynamics describing the flow of fluids could also describe the motion of cars along a road, provided a large-scale point of view is adopted so as to consider cars as small particles and their density as the main quantity to be looked at, see for instance [12]. The LWR model is a first-order model in the sense it is formulated as a scalar hyperbolic conservation law, and is often solved by finite difference methods (Daganzo, 1995; LeVeque, 1992; Lebacque, 1996). The LWR model is given by

$$\frac{\partial \rho}{\partial t} + \frac{\partial (\rho v)}{\partial x} = 0, \tag{1.1}$$

for $0 \leq \rho \leq \rho_{max}$, where ρ_{max} (also called jam density) is the value at which cars are bumper to bumper. Since the model is a scalar conservation law for ρ alone, the velocity v in (1.1) must be a given function of ρ (this is later discussed in details). Both Lighthill,

Whitham and Richards used the model (1.1) to demonstrate the existence of shockwaves in traffic systems. We will solve the Riemann problem of this model analytically and also produce some numerical solutions by implementing the first-order type Godunov approximation. This is proposed in this thesis to solve the LWR model because of the presence of discontinuities (shocks) in the solutions (Lebacque, 1996). Moreover, discontinuous weak solutions are not unique for hyperbolic conservation laws in general, hence entropy conditions [29] must be satisfied to obtain physically valid solution that is consistent with human behavior, such as the drivers ride impulse.

To address the limitations of this first order model, Lighthill and Whitham introduced a second-order model [15], but unfortunately, second order models for some time were not explored, until Payne and Whitham developed a second-order continuum model governing traffic flow. This new model is defined by the conservation of mass density (1.1) and the acceleration equation [2, 15] in which the average traffic speed v satisfies an evolution equation similar to the Navier-Stokes equation. This is written in nonconservative form as

$$\frac{\partial v}{\partial t} + v\frac{\partial v}{\partial x} \;=\; -\frac{p'(\rho)}{\rho}\frac{\partial \rho}{\partial x} + \frac{1}{\tau}\Big(V(\rho) - v\Big) + \frac{\mu}{\rho}\frac{\partial^2 v}{\partial x^2},$$

where τ and μ some positive constants, and a pressure law $p = p(\rho)$ inspired from gas dynamics. From the right side of this equation, the last term models viscosity or diffusion; it tends to adjust one's speed to that of the surrounding traffic, whereas the second term of expresses the tendency of traffic at a given density ρ to relax to some natural average speed $V(\rho)$ [19]. This is defined in such a way that, at low densities it is determined by road conditions and speed limits, and is only weakly dependent on ρ, whereas at high densities, $V(\rho)$ approaches zero, and is again weakly dependent on ρ. At intermediate densities it drops off rapidly, largely due to the fact that higher traffic density makes it more difficult for faster drivers to overtake slower drivers. Thus $V(\rho)$ is chosen to be decreasing function of the density ρ with a small derivative at low and high values of ρ, see for instance [19]. The first term is an anticipation factor; drivers slow down at the sight of an increase in traffic density ahead of them.

However, Daganzo [16] pointed out that traffic arriving at the end of a densely-packed queue would result in vehicles traveling backwards in space, which is physically unreasonable. This is due to the isotropic nature of the models, as the behavior of vehicles is influenced by vehicles behind them due to diffusive effects [16, 22]. Thus the Payne model, like other second-order models available in the literature, produced flawed behavior for some traffic conditions. These models violate the following principle: *a fluid particle responds to stimuli from the front and from behind a car is an anisotropic particle that mostly responds to frontal stimuli* [2]. To improve this model, Aw and Rascle [2] were able to produce an anisotropic second-order model which satisfies this principle, and averted the flaws noted by Dazgano by replacing the pressure term p in the momentum equation by an anticipation factor, i.e., a term which is supposed to describe how an average driver would react to a variation in the concentration of cars with respect to space. They concluded that the correct dependence of the pressure p on the density ρ must involve the *convective derivative*

$$\partial_t \;+\; v\partial x$$

of the pressure which will be still taken as an increasing function of the density

$$p \;=\; p(\rho).$$

Now assuming no diffusion and relaxation, the Aw-Rascle model is given as a coupled system of two equations presented here below

$$\begin{aligned} \partial_t \rho + \partial_x(\rho v) &= 0, \\ \partial_t\Big(v + p(\rho)\Big) + v\partial_x\Big(v + p(\rho)\Big) &= 0 \end{aligned} \tag{1.2}$$

with a prescribed initial data $U(x,0) := U_0 := (\rho_0, v_0)$ whose components are two bounded nonnegative functions. In this thesis we propose to consider the case where U_0 is defined by the following piecewise constant function:

$$U_0 = \begin{cases} U_\ell, & x < 0, \\ U_r, & x > 0. \end{cases} \tag{1.3}$$

Definition 1.1.1 The initial value problem for a conservative law (1.2) together with the piecewise constant data (1.3) having a single discontinuity is called the Riemann problem.

1.2 Outline of the Thesis

The thesis is organized in five more chapters that follow this introductory chapter. Chapter 2 reviews Hyperbolic systems of conservation laws by giving some basic backgrounds, Chapter 3 discusses the first order fluid approximation of traffic flow dynamics proposed by Lighthill and Witham and Richard: the LWR model that provides a coarse description of traffic behavior for a single one-way road using three variables that vary in time and space: flow, q, density, ρ, and speed, v. Chapter 4 is devoted to the Aw and Rascle (shortly Aw-Rascle) model of traffic flow. This describes the evolution of traffic flow via a coupled system of mass conservation and momentum balance equations. These two later chapters account mainly for traffic models on single one-way roads. Chapter 5 reports about the comparison of the LWR and Aw-Rascle models. Finally, chapter 6 concludes this thesis.

Chapter 2

Hyperbolic Systems of Conservation Laws

This chapter reviews hyperbolic systems of conservation laws. For more details we refer the reader to [8, 9]. We discuss time-dependent systems of partial differential equations of the general following form

$$\frac{\partial u}{\partial t} + \frac{\partial f(u)}{\partial x} \quad = \; 0, \tag{2.1}$$

with $u \;:\; \mathbb{R} \times \mathbb{R} \rightarrow \;\mathbb{R}^m$ an $m-$dimensional vector of conserved quantities, or state variables, such mass, momentum, and energy appearing in a problem, for instance, fluid dynamics [9] or traffic flow problems. In the study of hyperbolic Systems of conservation laws the main assumption is that knowing the value of $u(x,t)$ at a given point and time allows us to determine the rate of flow, also called as **flux**, of each state variable at point (x,t). In our notations, $f \;:\; \mathbb{R}^m \;\rightarrow\; \mathbb{R}^m$ is called the **flux function** for the system of conservation laws.

Definition 2.0.1 The system (2.1) is **hyperbolic** if the Jacobian matrix $f'(u)$ of the flux function has the following property: for each value of u the eigenvalues of $f'(u)$ are real, and the matrix is diagonalizable, i.e., there is a complete set of m linearly independent eigenvectors.

Let $\psi \in \mathcal{C}_0^1(\mathbb{R} \times \mathbb{R}^+)$ be a test function, with $\mathcal{C}_0^1$ the space of functions that are continuously differentiable with compact support. If we multiply the system (2.1) by this test function ψ and then integrate over space and time, we get

$$\int_0^\infty \int_{-\infty}^{\infty} \Big[\psi_t u + \psi_x f(u)\Big] dxdt \;\; = \;\; -\int_{-\infty}^{\infty} \psi(x,0)u(x,0)dx. \tag{2.2}$$

Definition 2.0.2 *The function $u(x,t)$ is called a weak solution of the system (2.1) if (2.2) holds for all functions $\psi \in \mathcal{C}_0^1(\mathbb{R} \times \mathbb{R}^+)$.*

2.0.1 Godunov Scheme for Nonlinear Conservation laws

In 1959, Godunov proposed a way to make use of the characteristic information within the framework of a conservative method. Rather than attempting to follow characteristics

backwards in time, Godunov suggested solving Riemann problems forward in time. This scheme is similar to the Upwind scheme. We refer the reader to the literature, see for instance [1, 4, 9]. Now consider the following initial value problem

$$\begin{aligned} \frac{\partial u}{\partial t} + \frac{\partial f(u)}{\partial x} &= 0, \qquad & x \in \mathbb{R}, \quad t \in \mathbb{N}, \\ u(x,0) &= u_0(x), \qquad & \forall x \in \mathbb{R}. \end{aligned} \tag{2.3}$$

Define

$$x_{j+\frac{1}{2}} \;=\; x_j + \frac{h}{2},$$

with h the mesh width. The Godunov scheme will produce approximations $U^n \in \mathbb{R}^m$ to a cell average of $u(x, t_n)$ defined by

$$\bar{u}_j^n \;=\; \frac{1}{h}\int_{x_{j-\frac{1}{2}}}^{x_{j+\frac{1}{2}}} u(x,t_n)dx.$$

- Use the given initial data $u_0(x)$ and define the initial data U^0 for our numerical method by $U_j^0 \;=\; \bar{u}_j^0$.
- Now use a time-marching procedure to construct the approximation U^1 from U^0, then U^2 from U^1 and so on. In general we construct U^{n+1} from U^n, for $n \in \mathbb{N}$.
- Use the numerical solution U^n to define a piecewise constant function $\tilde{u}^n(x, t_n)$ with the value U_j^n on the grid cell $x_{j-\frac{1}{2}} \;<\; x \;<\; x_{j+\frac{1}{2}}$.
- Next, use $\tilde{u}^n(x, t_n)$ as initial data of the conservation law, which is solved exactly to obtain $\tilde{u}^n(x, t)$ for $t_n \;\leq\; t \;\leq\; t_{n+1}$. Here use a short time interval since the initial data $\tilde{u}^n(x, t_n)$ is piecewise constant.
- Hence define a sequence of Riemann problems.
- Piece these Riemann solutions together to obtain the exact solution up to the time when waves from neighboring Riemann problems begin to interact. Hence we obtain the exact solution over the time interval $[t_n, t_{n+1}]$.
- Now define the approximate solution U^{n+1} at time t_{n+1} by averaging this exact solution at time t_{n+1}, this yields

$$U_j^{n+1} \;=\; \frac{1}{h}\int_{x_{j-\frac{1}{2}}}^{x_{j+\frac{1}{2}}} \tilde{u}(x,t_{n+1})dx. \tag{2.4}$$

  Use these values to define new piecewise constant data $\tilde{u}^{n+1}(x, t_{n+1})$ and repeat the process.

The cell average (2.4) can be easily computed using the integral form of the conservation law [9]. Since $\tilde{u}^n$ is assumed to be an exact weak solution, we have

$$\int_{x_{j-\frac{1}{2}}}^{x_{j+\frac{1}{2}}} \tilde{u}(x,t_{n+1})dx \;=\; \int_{x_{j-\frac{1}{2}}}^{x_{j+\frac{1}{2}}} \tilde{u}(x,t_n)dx + \int_{t_n}^{t_{n+1}} f\Big(\tilde{u}^n(x_{j-\frac{1}{2}},t)\Big)dt - \int_{t_n}^{t_{n+1}} f\Big(\tilde{u}^n(x_{j+\frac{1}{2}},t)\Big)dt.$$

Note that $\tilde{u}^n(x,t_n) \;=\; U^n$ over the cell $(x_{j-\frac{1}{2}}, x_{j+\frac{1}{2}})$. Dividing (2.5) by h yield

$$U_j^{n+1} \;=\; U_j^n - \frac{k}{h}\Big[F\Big(U_j^n, U_{j+1}^n\Big) - F\Big(U_{j-1}^n, U_j^n\Big)\Big] \tag{2.5}$$

with F the numerical flux defined by

$$F\Big(U_j^n, U_{j+1}^n\Big) \;=\; \frac{1}{k}\int_{t_n}^{t_{n+1}} f\Big(\tilde{u}^n(x_{j+\frac{1}{2}},t)\Big)dt. \tag{2.6}$$

Remark that the solution of the Riemann problem at the point $x_{j+\frac{1}{2}}$ is a similarity solution, which is constant along each ray $\Big(x - x_{j+\frac{1}{2}}\Big)/t \;=\;$ constant. Therefore $\tilde{u}^n$ is constant at $x_{j+\frac{1}{2}}$ over the time interval $\Big(t_n, t_{n+1}\Big)$, which simplifies the integral in (2.6).

Denote $u^*(U_j^n, U_{j+1}^n)$ the constant value of $\tilde{u}^n$ along the line $x \;=\; x_{j+\frac{1}{2}}$, then the flux defined in (2.6) becomes

$$F\Big(U_j^n, U_{j+1}^n\Big) \;=\; f\Big(u^*(U_j^n, U_{j+1}^n)\Big). \tag{2.7}$$

We simplify our notation by using

$$F_{j+\frac{1}{2}} \;=\; F\Big(U_j^n, U_{j+1}^n\Big), \quad \text{and} \;\; F_{j-\frac{1}{2}} \;=\; F\Big(U_{j-1}^n, U_j^n\Big). \tag{2.8}$$

Proposition 2.1 *The Godunov method can be written in conservative form*

$$U_j^{n+1} \;=\; U_j^n - \frac{k}{h}\Big[F_{j+\frac{1}{2}} - F_{j-\frac{1}{2}}\Big], \tag{2.9}$$

with intercell numerical flux given by (2.8)*, if the time step k satisfies the following condition*

$$k \;\leq\; \frac{h}{\lambda_{max}^n}, \tag{2.10}$$

where λ_{max}^n denotes the maximum wave velocity at time t^n. For the proof of this proposition we refer the reader to [10].

2.0.2 The CFL Condition

In our numerical aspects, a necessary but not sufficient condition for the stability is going to be the CFL (Courant, Friedrichs, and Lewy) condition [9, 10]. The idea is to define a sequence of approximate solutions via finite difference equations, prove that they converge as the grid is refined, and then show that the limit function must satisfy the partial differential equation, giving existence of a solution, see e.g. [1, 9, 10] for more details. The CFL condition is given by (2.10) above.

2.0.3 Consistency of the Godunov Method

Definition 2.0.3 We call the method (2.9) **consistent** with the original conservation law if the numerical flux F reduces to the true flux f for the case of constant flow, i.e.,

$$F(U, ..., U) = f(U) \qquad \forall U \in \mathbb{R}.$$

Now let $U_j^n = U_{j+1}^n \equiv \bar{u}$, then since $u^*(U_j^n, U_{j+1}^n)$ depends only on the data U_j^n and U_{j+1}^n we get $u^*(U_j^n, U_{j+1}^n) = \bar{u}$. Hence the Godunov flux F is consistent with f [9]. Here we require some smoothness idea, so that as the two arguments F approach some common value $\bar{u}$, the value of F approaches $f(\bar{u})$ in a smooth maner. For consistency it is sufficient to have F a Lipschtz continuous function of each variable. By definition, F is said to be Lipschitz at a point $\bar{u}$ if there exists a constant $C \geq 0$ such that, for all v, w with $|v - \bar{u}|$ and $|w - \bar{u}|$ sufficiently small, the following inequality holds:

$$|F(v, w) - f(\bar{u})| \leq C\max(|v - \bar{u}|, |w - \bar{u}|)$$

If F is Lipschitz at every point $u \in \mathbb{R}$, then it is a Lipschitz continuous function.

Theorem 2.0.1 *(Kruscov)*
The scalar initial value problem

$$\begin{aligned} u_t + f(u)_x &= 0, \quad f \in \mathcal{C}^1(\mathbb{R}) \\ u(x, 0) &= u_0(x), \quad u_0 \in \mathcal{L}^\infty(\mathbb{R}) \end{aligned}$$

has a unique entropy [9] solution $u \in \mathcal{L}^\infty(\mathbb{R} \times \mathbb{R})$. This solution has the following properties:

i) $\mathcal{L}^\infty$ stability property:

$$\Big|\Big|u(\cdot, t)\Big|\Big|_\infty \leq \Big|\Big|u_0(\cdot)\Big|\Big|_\infty$$

ii) Monotonicity property:

$$u_0(\cdot) \geq v_0(\cdot) \quad \Rightarrow \quad u(\cdot, t) \geq v(\cdot, t)$$

iii) The total variation (TV) is conserved. *Let BV denotes the space of functions with bounded total variation. Then the following remains true for any time t in$\mathbb{R}^+$:*

$$u_0(\cdot) \in BV \quad \Rightarrow \quad u(\cdot, t) \in BV$$

in other words, $TV(u_0) \geq TV(u(\cdot, t))$. The total variation can neither increase nor decrease in time.

iv) Conservation property:

$$\begin{aligned} u_0 \in \mathcal{L}^1(\mathbb{R}) \quad &\Rightarrow \quad \int_{\mathbb{R}} u(x,t)dx \\ &= \quad \int_{\mathbb{R}} u_0(x)dx, \quad t \in \mathbb{R}^+. \end{aligned}$$

For more details we refer the reader to [30, 31, 34].

Chapter 3

The LWR Model and Its Numerical Solutions

To describe the dynamic characteristics of traffic on a homogeneous and unidirectional highway, Lighthill and Whitham (1955) and Richards (1956) independently proposed a first order fluid approximation of traffic flow dynamics, known as LWR model in the literature of traffic flow theory. This model describes the behavior of the traffic for a single one-way road using three variables that vary in time and space: flow, q, density, ρ, and speed, v. The LWR is a basic linear ordinary differential equation model of traffic flow that incorporates the idea of equilibrium flow rate. Because of its simplicity and good explanatory power to understand the qualitative behavior of road traffic, it is still widely used for the modeling of traffic flow even if advances have been made in many directions. The results that are obtained from the LWR model are generally adequate for many applications such as traffic management and control problems [17]. As we have already said in the introductory chapter, the model does not contain any inertial effects, which implies that the vehicles adjust their speeds instantaneously, nor does it contain any diffusive terms, which would model the ability of drivers to look ahead and adjust to changes in traffic conditions, such as shocks, before they arrive at the vehicle itself.

3.1 Description of the Mathematical Model

Let us consider a car moving along a highway. Let $x \in \mathbb{R}$ be the coordinate along this highway, and $t \in \mathbb{R}^+$ a time coordinate. In our notations, $q = q(x,t)$ stands for the flow rate or flux, i.e., the average number of cars passing per time unit, and $\rho = \rho(x,t)$ denotes the density of cars, that is, the number of cars per unit length. Now consider the flow of cars on a highway without slip-roads and exits so that the model will conserve vehicles. Let us fix a certain section $[x_1, x_2]$ on this highway and two quite close times $t_1 < t_2$. Since we have assumed no slip-roads and exits there exists no car sources. Therefore, no cars are created or destroyed in the interval $[x_1,\ x_2]$, then the changes in the number of cars result from crossings at $x = x_1$ and $x = x_2$ only. We deduce that the same cars entered from the point x_1 at a certain time will exit from the point x_2. Thus the difference of the the total quantity of cars in the segment between the two considered instants must be equal to the difference of the total flux at the endpoints

$$\int_{x_1}^{x_2} \Big(\rho(x,t_2) - \rho(x,t_1)\Big)dx \;=\; \int_{t_1}^{t_2} \Big(q(x_1,t) - q(x_2,t)\Big)dt. \tag{3.1}$$

Now assume that ρ and q are regular (analytic and single-valued) functions in the considered interval. Dividing the integrals (3.1) by the product $(x_2 - x_1)(t_2 - t_1)$ and taking the limits $x_2 - x_1 \rightarrow 0$ and $t_2 - t_1 \rightarrow 0$, we finally obtain the conservation law:

$$\frac{\partial \rho(x,t)}{\partial t} + \frac{\partial q(x,t)}{\partial x} = 0, \tag{3.2}$$

In our further notations we would like to use the subscript t to replace the partial derivative with respect to time t, and subscript x to replace the partial derivative with respect to location x. The LWR theory proposed that the relation between flow and density observed under steady state conditions also holds when flow and density vary with x and t, i.e., for a homogenous highway:

$$q = Q\Big(\rho(x,t)\Big),$$

where Q is a differentiable positive function of the density defined such that the flow increased with increasing vehicle density until a maximum was reached, and decreased to zero as the density increased further. Thus Q takes the form

$$Q(\rho) = \rho V, \tag{3.3}$$

Substituting (3.3) into (3.2) gives

$$\rho_t + (\rho V)_x = 0, \tag{3.4}$$

which is the differential form of the conservation of density ρ, also known as continuity equation, which relates the local traffic density ρ to the local average speed $v(\rho)$ of the cars. In order to obtain a scalar conservation law for density ρ alone, the average speed V at any point of the road was defined as a regular strictly decreasing function of ρ:

$$V = V(\rho),$$

which makes sense since on a highway we would optimally like to drive at some speed v_{max}, the maximum speed, but in a heavy traffic we slow down with velocity decreasing to 0 as the density ρ approaches some fixed maximal density ρ_{max}. Lighthill and Whitham and independently Richards proposed this type of mathematical model of traffic flow. If there are no other cars on the highway corresponding to very low traffic densities or free flow, then the car would travel at the maximum speed v_{max},

$$V(0) = v_{max}.$$

The maximal speed v_{max} is sometimes referred to as the "mean free speed" corresponding to the velocity that cars would travel if they were free from interference from other cars. At a certain density cars stop before they touch to each other. This maximum density, ρ_{max}, usually corresponds to what is called bumper-to-bumper traffic or jam density:

$$V(\rho_{max}) \;=\; 0.$$

Lighthill and Whitham proposed a simple, but qualitatively reasonable linear dependence of $V(\rho)$ and ρ given by the following linear relation:

$$V(\rho) \;=\; v_{max}\Big(1-\frac{\rho}{\rho_{max}}\Big), \tag{3.5}$$

then the flux in (3.3) takes the form

$$q(\rho) = \rho v_{max}\Big(1-\frac{\rho}{\rho_{max}}\Big).$$

From this we expect to drive at the maximum speed v_{max} when the road is empty, but as long as ρ approaches the maximal value ρ_{max} when the cars are bumper-to-bumper density we slow down to zero velocity.

Substituting (3.5) into (3.4) yields

$$\rho_t + \Big(\rho v_{max}\Big(1-\frac{\rho}{\rho_{max}}\Big)\Big)_x \;=\; 0. \tag{3.6}$$

This expression is known as LWR model.

Now define the flux function

$$f(\rho) \;=\; \rho v_{max}\Big(1-\frac{\rho}{\rho_{max}}\Big), \tag{3.7}$$

then the model (3.6) takes the general form

$$\rho_t + \Big(f(\rho)\Big)_x \;=\; 0, \quad x\in\mathbb{R},\ t\in\mathbb{R}^+. \tag{3.8}$$

Obviously, $f''(\rho)<0$, thus f is concave. The characteristic speeds for (4.11) with flux (3.7) are given by

$$f'(\rho) \;=\; v_{max}\Big(1-\frac{2\rho}{\rho_{max}}\Big)$$

Note that, depending on the value of density, characteristic speeds can be either positive ($\forall\rho<\frac{\rho_{max}}{2}$) or negative ($\forall\rho>\frac{\rho_{max}}{2}$). They are zero if $\rho=\frac{\rho_{max}}{2}$.

From (3.8) discontinuities can develop in finite time $t\in[0,\ T]$, even from smooth initial data (Lax, 1972). One therefore has to expand the class of solutions of hyperbolic PDEs such as (3.8) to include discontinuous solutions. These discontinuous solutions are called shock waves. On either side of a shock, the solution $\rho(x,t)$ satisfies the differential equation (3.8) in the classical sense, i.e., derivatives appearing in this equation: ∂_t and ∂_x are continuous. Along the path of the shock $X_s(t)$, however, the discontinuous states ρ_ℓ,ρ_r satisfies the so-called *Rankine-Hugoniot jump condition*:

$$s[\rho] \;=\; [f(\rho)], \tag{3.9}$$

where

$$[g(\rho)] \;:=\; g(\rho_\ell) - g(\rho_r),$$

is the jump of the function $g(\rho)$ across the discontinuity (shock) and $s = \dot{X}_s(t)$ is the shock speed, ρ_ℓ and ρ_r are the values of the density at the location to the left and right of the shock, respectively. Furthermore, among the possible shocks whose speed satisfies the Rankine Hugoniot jump condition, only those that absorb characteristics from both sides of the shock path are admissible, i.e., the admissible shocks must satisfy the so called *entropy condition*

$$f'(\rho_\ell) > \;\; s > \;\; f'(\rho_r) \tag{3.10}$$

Moreover, $s < f'(\rho_\ell) < v$, cars therefore enter the shock from left (behind) and drop speed abruptly after crossing the shock. On the other hand, if $\rho_\ell > \rho_r$ a smooth solution, called a rarefaction wave can be obtained from

$$f'\Big(\rho(\beta)\Big) \;\; = \;\; \beta, \qquad \beta \;=\; x/t;$$

or

$$\rho(\beta) \;\; = \;\; \Big(f'\Big)^{-1}\Big(\beta\Big), \qquad f'(\rho_\ell) < \beta < f'(\rho_r).$$

We summarize this in the next sections; we discuss these two types of solutions mentioned above in details, we will also discuss numerical solutions of the LWR model on one-lane highway in the last section.

3.2 Analytical Solution of the LWR Model

Now let us turn our discussions to the Riemann problem for the LWR model (4.11) and present the analytical solutions of this model. As we have already said, depending on the choice of initial data we distinguish two types of solutions of the model, in general; these are Lax-shock wave solution as well as rarefaction wave. In this section we discuss the details of these solutions.

3.2.1 The Riemann Problem of the LWR Model

Consider the LWR model defined in (3.8) with the following piecewise constant initial condition:

$$\rho(x,0) \;\; = \;\; \begin{cases} \rho_\ell, & x < 0, \\ \rho_r, & x > 0. \end{cases} \tag{3.11}$$

where ρ_ℓ and ρ_r are the values of the density ρ on the left and right side of the discontinuity at the point $x = 0$ respectively. The behavior of the solution $\rho(x,t)$ at some time $t > 0$ depends on the relation between these two initial states ρ_ℓ and ρ_r. To determine the analytical solutions of the Riemann problem of the LWR model defined by (3.8) with

Riemann data (3.11) and flow flux function f defined by (3.3), we start by differentiating this equation to obtain

$$f'(\rho) \;=\; v_{max}\Big(1-\frac{2\rho}{\rho_{max}}\Big). \tag{3.12}$$

This expression gives the characteristic speeds for the LWR model (3.8). This equation, together with the entropy condition (3.10) imply that $\rho_\ell < \rho_r$, that is, the upstream traffic density is lower. Hence in this case the solution $\rho(x,t)$ at some given time $t > 0$ will be a shock wave satisfying the Lax-entropy condition (3.10). In the opposite case, i.e., when $\rho_\ell > \rho_r$ we will have a rarefaction wave. Hence depending on the values of the Riemann data, we distinguish the following two types of solutions for the LWR model:

Case I: $0 < \rho_\ell < \rho_r < \rho_{max}$

This is the case when the upstream traffic density is lower. In this case there is a unique entropy shock wave solution which satisfies the entropy condition (3.10), and is given by

$$\rho(x,t) = \begin{cases} \rho_\ell, & x \le st, \\ \rho_r, & x > st. \end{cases} \tag{3.13}$$

where s defines the shock speed and is computed from the Rankine Hugoniot condition (3.9). Hence

$$s \;=\; v_{max}\Big(1-\Big(\frac{\rho_\ell+\rho_r}{\rho_{max}}\Big)\Big) \tag{3.14}$$

is the speed at which the discontinuity will propagate. The shock may either propagate to the left if $s < 0$, or to the right if $s > 0$, depending on how the Riemann data ρ_ℓ and ρ_r are chosen.

Case II: $0 < \rho_r < \rho_\ell < \rho_{max}$

In this case the solution is a similarity solution, i.e., solution that is a function of x/t alone. This is usually known as a continuous rarefaction wave solution given by

$$\rho(x,t) \;=\; \begin{cases} \rho_\ell, & x/t \le \beta_1, \\ w(x/t), & \beta_1 < x/t < \beta_2, \\ \rho_r, & x/t \ge \beta_2, \end{cases} \tag{3.15}$$

where w is a smooth function with $w(\beta_1) \;=\; \rho_\ell$ and $w(\beta_2) \;=\; \rho_r$. The explicit function $w(x/t)$ in the above expression is determined in the following procedure:

Set $\rho(x,t) \;=\; w(x/t)$, and differentiate with respect to t and x, to obtain

$$\begin{aligned} \rho_t(x,t) &= -\frac{x}{t^2}w'(x/t), \\ \rho_x(x,t) &= -\frac{1}{t}w'(x/t). \end{aligned} \tag{3.16}$$

Substituting (3.16) into (3.8) we get

$$-\frac{x}{t^2}w'(x/t) + \frac{1}{t}f'\Big(w(x/t)\Big)w'(x/t) \;=\; 0.$$

We multiply this equation by t and rearrange the terms to obtain

$$f'\Big(w(\beta)\Big)w'(\beta) \;=\; \beta w'(\beta), \tag{3.17}$$

from which we can determine $w(\beta)$ uniquely; here $\beta = x/t$ as before. The solution ρ is constant along all rays of the form $x = \beta t$. Solving equation (3.17) gives two solutions: one possible solution is $w'(\beta) \equiv 0$, i.e., w is constant. Any constant function satisfies (3.8), therefore, is its similarity solution. Indeed the rarefaction wave takes this form for $\beta \leq \beta_1$ and $\beta \geq \beta_2$. For $\beta_1 < \beta < \beta_2$, w is smoothly varying and $w' \neq 0$. Hence From (3.17) we see that w solves

$$f'\Big(w(\beta)\Big) \;=\; \beta, \qquad\qquad \beta_1 < \beta < \beta_2, \tag{3.18}$$

which yields, using (3.12)

$$v_{max}\Big(1 - \frac{2w}{\rho_{max}}\Big) \;=\; \beta,$$

and finally

$$w(\beta) \;=\; \frac{\rho_{max}}{2}\Big(1 - \frac{\beta}{v_{max}}\Big).$$

With this, the rarefaction wave (3.16) takes the form

$$\rho(\beta) \;=\; \begin{cases} \rho_\ell, & \beta \leq f'(\rho_\ell), \\ w(\beta), & f'(\rho_\ell) < \beta < f'(\rho_r), \\ \rho_r, & \beta \geq f'(\rho_r). \end{cases} \tag{3.19}$$

3.3 Numerical Solution Method for the LWR Model

In order to solve the LWR model numerically we propose to use the Godunov method that is discussed in this section. We know from [9], that the Godunov (1959) method is sufficient for solving hyperbolic systems of conservation laws. For the LWR model, therefore, we use the Godunov-type difference equations to approximate it.

For our numerical simulations, we discretize the $x - t$ plane by choosing, for simplicity, a uniform mesh width $h \;=\; \Delta x$ in the scaled interval $[-4, 4]$, and a time step $k \;=\; \Delta t$ in the scaled interval $[0, 3]$. Define the discrete mesh points (x_i, t_n) by

$$\begin{aligned} x_i \;&=\; ih, \qquad i \;=\; ..., -1, 0, 1, 2, ... \\ t_n \;&=\; nk, \qquad n \;=\; 0, 1, 2, ... \end{aligned}$$

We discretize the time derivative using the forward differencing. Define the control volumes or cells V_j as follows:

$$V_j = \Big[x_{j-\frac{1}{2}}, x_{j+\frac{1}{2}}\Big), \qquad x_{j+1/2} = x_j + \frac{h}{2}, \quad j = 0, \pm 1, \pm 2, ...$$

Let $\bar{\rho}(x,t)$ be the solution of the following Riemann problem

$$\bar{\rho}_t + v_{max}\Big(\bar{\rho}\Big(1 - \frac{\bar{\rho}}{\rho_{max}}\Big)\Big)_x = 0, \quad -\infty < x < \infty, \;\; t > t^n, \tag{3.20}$$

with initial value, i.e., the density at t^n

$$\bar{\rho}(x, t^n) = \begin{cases} \rho_j^n, & x < x_{j+\frac{1}{2}}, \\ \rho_{j+1}^n, & x > x_{j+\frac{1}{2}}. \end{cases}$$

The solution of this Riemann problem is a similarity of the form

$$\bar{\rho}(x,t) = \rho_R\Big(\beta; \rho_j^n, \rho_{j+1}^n\Big), \quad \beta = \frac{x - x_{j+\frac{1}{2}}}{t - t^n}.$$

Clearly, $\beta = 0$ for $x = x_{j+\frac{1}{2}}$, hence the numerical flux is defined by

$$F\Big(\rho_j^n, \rho_{j+1}^n\Big) = f\Big(\rho_R\Big(0; \rho_j^n, \rho_{j+1}^n\Big)\Big) \tag{3.21}$$

where $f(\bar{\rho})$ is the flux function and can be easily obtained from (3.20)

$$f(\bar{\rho}) = \bar{\rho} v_{max}\Big(1 - \frac{\bar{\rho}}{\rho_{max}}\Big). \tag{3.22}$$

We obtain the following numerical fluxes:

- For $\rho_j^n < \rho_{j+1}^n$, the solution is a shock wave moving with speed s_j^n defined by

$$s_j^n = v_{max}\Big[1 - \frac{1}{\rho_{max}}\Big(\rho_j^n + \rho_{j+1}^n\Big)\Big]$$

  and the numerical flux reduces to

$$F\Big(\rho_j^n, \rho_{j+1}^n\Big) = \begin{cases} \rho_j^n v_j^n, & 0 < s_j^n, \\ \rho_{j+1}^n v_{j+1}^n, & 0 > s_j^n. \end{cases}$$

  Here we denote V_j^n for the velocity at time t^n on the left side of the discontinuity:

$$v_j^n = v_{max}\Big(1 - \frac{\rho_j^n}{\rho_{max}}\Big).$$

- On the other hand, for $\rho_j^n > \rho_{j+1}^n$, we have a rarefaction wave and the numerical flux is given by

$$F\Big(\rho_j^n, \rho_{j+1}^n\Big) = \begin{cases} \rho_j^n v_j^n, & 0 < \lambda_j^n, \\ \frac{1}{4}\rho_{max} v_{max}, & \lambda_j^n < 0 < \lambda_{j+1}^n, \\ \rho_{j+1}^n v_{j+1}^n, & \lambda_{j+1}^n > 0, \end{cases}$$

with

$$\begin{aligned} \lambda_j^n &= f'(\rho_j^n) \\ &= v_{max}\Big(1 - 2\frac{\rho_j^n}{\rho_{max}}\Big). \end{aligned}$$

With the above numerical flux we define the Godunov scheme for LWR model by

$$\rho_j^{n+1} = \rho_j^n - \frac{k}{h}\Big[F\Big(\rho_{j+1}^n, \rho_j^n\Big) - F\Big(\rho_{j-1}^n, \rho_j^n\Big)\Big]. \tag{3.23}$$

We now need to specify the CFL (Courant Friedrichs and Lewy) condition for the stability of our numerical solutions. This is already defined in (2.10) in the introductory chapter. In our numerics we chose

$$\Big|\frac{\Delta t}{\Delta x} f'\Big(\rho_j^n\Big)\Big| = 0.99,$$

that is,

$$\Big|\frac{\Delta t}{\Delta x} v_{max}\Big(1 - 2\frac{\rho_j^n}{\rho_{max}}\Big)\Big| = 0.99.$$

for all ρ_j^n. Note that the value $v_{max}\Big(1 - 2\frac{\rho_j^n}{\rho_{max}}\Big)$ is always bounded from above by v_{max} for any value of ρ_j^n. Therefore, Δt is chosen to be

$$\Delta t = 0.99 \times \Delta x / v_{max}.$$

3.3.1 Numerical Examples

We present different choices of Riemann data that lead us to both shock and rarefaction waves. We start with simple computations under the assumptions: $\rho_{max} = 1$ and $v_{max} = 1$, and then later we discuss a more realistic problem where the highway will be considered in km and the maximum velocity v_{max} chosen in km/h.

(i) Simple Case

Now let $\rho_{max} = 1$ and $v_{max} = 1$. We assume the uniform grid spacing with step size $h = 0.01$, for space and Δt for time is deduced from the CFL condition defined above. Hence $\Delta t = 99 \times 10^{-4}$, since $v_{max} = 1$.

Initial condition 3.1 Consider an end of the traffic with stationary cars on the right, i.e., $v_r = 0$. The corresponding initial condition is given by

$$\rho(x,0) = \begin{cases} 0.4, & x < 0, \\ 1, & x > 0. \end{cases} \tag{3.24}$$

The corresponding exact solution to this Riemann problem is a shock wave moving at speed $s = -0.4$ and propagates to the left. From (3.5) we have a positive speed of cars from the left, $v_\ell = 0.6$, and stationary cars on the right, i.e., $v_r = 0$. This models the situation in which cars moving at positive speed of 0.6 from the left unexpectedly encounter a bumper-to-bumper traffic jam and slam on their brakes, instantaneously reducing their velocity to 0, while the density jumps from 0.4 to 1. This discontinuity occurs at the shock, and clearly the shock location moves to the left as more cars join the traffic jam. From the numerical results of this problem we observe that the exact shock computed in (3.13) is well captured by our numerical scheme with the refined mesh size, in our case $\Delta x = 0.01$. See the numerical results plotted in Figure 3.1.

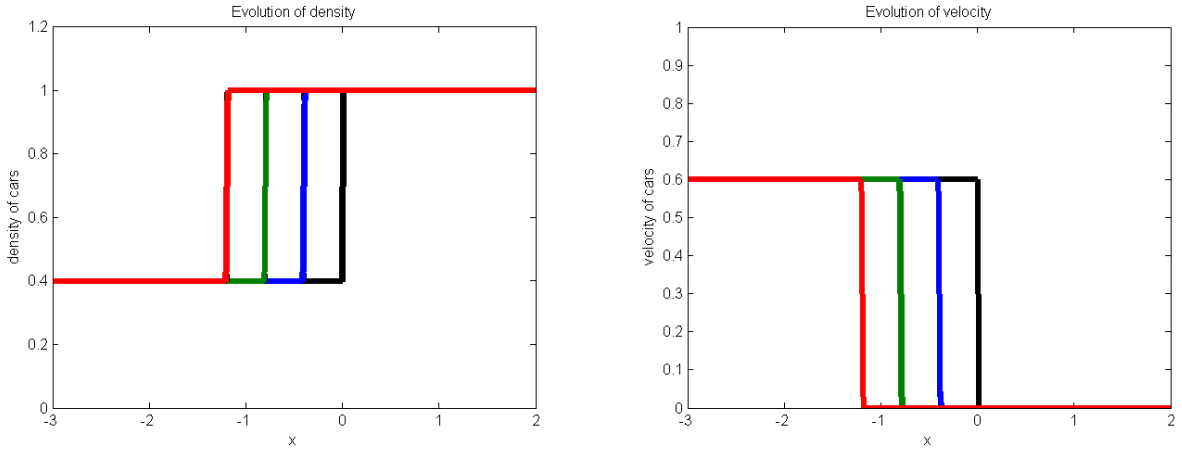

(a) Evolution of density

(b) Evolution of velocity

Figure 3.1: *Solution of the LWR model with data $\rho_\ell = 0.4$ and $\rho_r = 1$. Here the black solid line is the initial state, the blue line represents the solution at $t = 1$, the green line is the solution at $t = 2$, and the red line is the solution at $t = 3$. The dashed-lines are the corresponding exact solutions.*

Initial condition 3.2 Now let us consider the following initial value

$$\rho(x,0) = \begin{cases} 0.2, & x < 0, \\ 0.6, & x > 0. \end{cases} \tag{3.25}$$

Since $\rho_\ell < \rho_r$, the exact solution to this Riemann problem is again a shock wave but moving forward with positive speed $s = 0.2$. The numerical results are presented in Figure 3.2.

Initial condition 3.3 We now turn to the rarefaction case where cars are more concentrated on the left side of the discontinuity. We start with the initial state

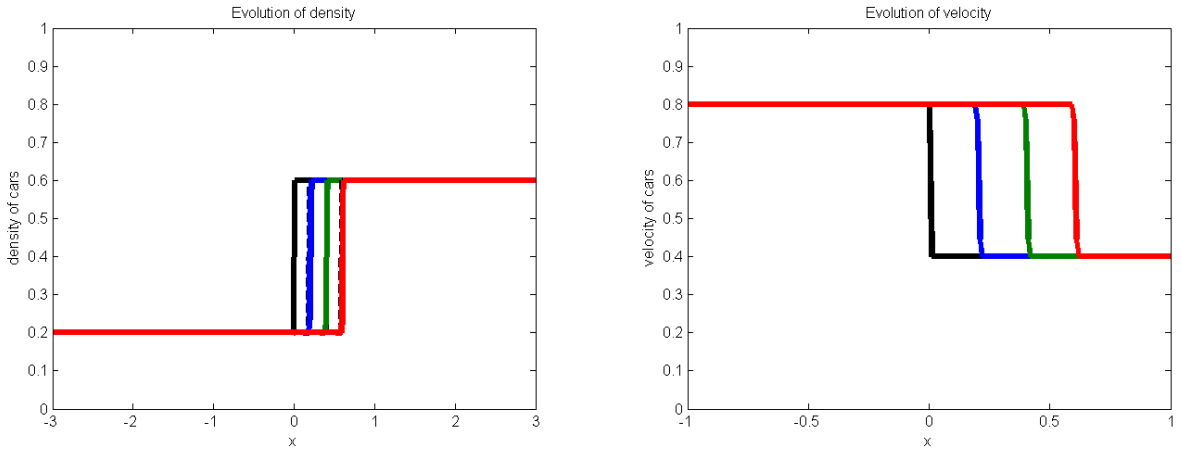

(a) Evolution of density

(b) Evolution of velocity

Figure 3.2: *Solution of the LWR model with data* $\rho_\ell = 0.2$ *and* $\rho_r = 0.6$. *Here the black solid line is the initial state, the blue line represents the solution at* $t = 1$, *the green line is the solution at* $t = 2$, *and the red line the solution at* $t = 3$. *The dashed-lines are the corresponding exact solutions.*

$$\rho(x,0) = \begin{cases} 1, & x < 0, \\ 0.5, & x > 0. \end{cases} \tag{3.26}$$

This state model the situation in which cars start moving a light turns green. In this situation we obtain from (3.5), the velocity $v_\ell = 0$ and $v_r = 0.5$. This means that cars located to the left are initially stationary but can begin to accelerate once the cars in front of them begin to move. The exact solution of this problem is a left-going rarefaction wave of the form discussed in (3.19) and the corresponding numerical solutions are shown in Figure 3.3.

Initial condition 3.4 Consider the initial state

$$\rho(x,0) = \begin{cases} 0.8, & x < 0, \\ 0.2, & x > 0. \end{cases} \tag{3.27}$$

Here we again have for the exact solution to this Riemann problem, a rarefaction wave going to the left with speed $f'(\rho_\ell) = -0.6$ and to the right with speed $f'(\rho_r) = 0.6$. See Figure 3.4 for the numerical results.

Initial condition 3.5 Here the tail of a group of moving cars following an empty road in front is studied. We set the initial data as

$$\rho(x,0) = \begin{cases} 0.5, & x < 0, \\ 0, & x > 0. \end{cases} \tag{3.28}$$

The exact solution of this Riemann problem is a right-going rarefaction wave. See Figure 3.5 for both exact (dashed-lines) and numerical solutions.

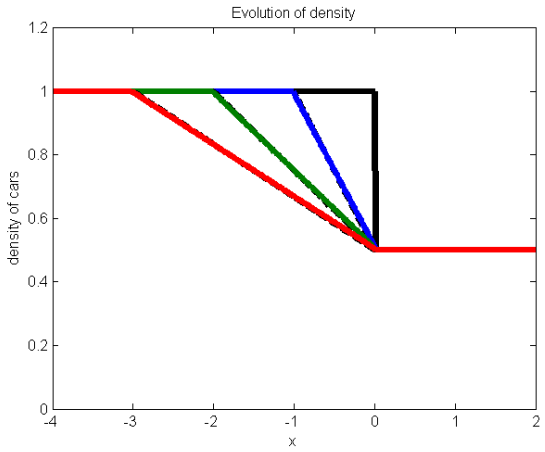

(a) Evolution of density

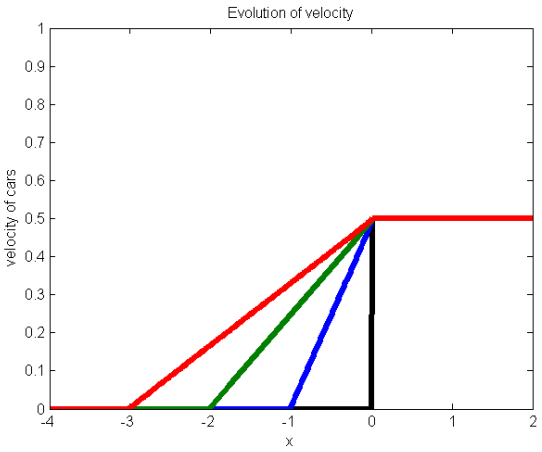

(b) Evolution of velocity

Figure 3.3: *Solution of the LWR model with data* $\rho_\ell = 1$ *and* $\rho_r = 0.5$. *Here the black solid line is the initial state, the blue line represents the solution at* $t = 1$, *the green line is the solution at* $t = 2$, *and the red line the solution at* $t = 3$. *The dashed-lines are the corresponding exact solutions.*

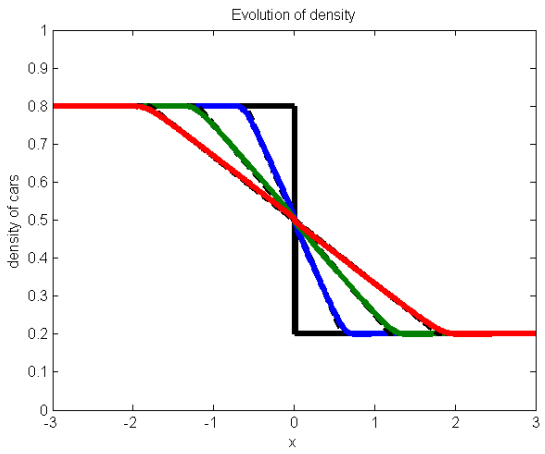

(a) Evolution of density

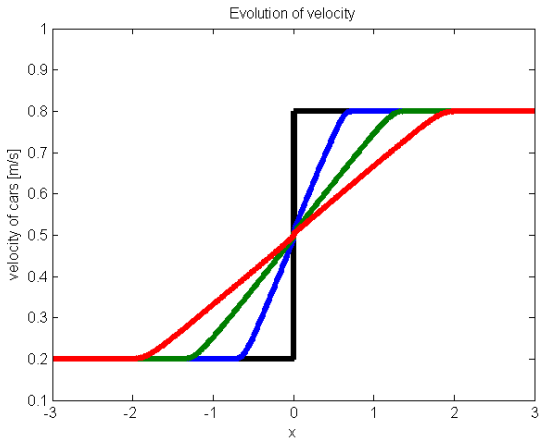

(b) Evolution of velocity

Figure 3.4: *Solution of the LWR model with data* $\rho_\ell = 0.8$ *and* $\rho_r = 0.2$. *Here the black solid line is the initial state, the blue line represents the solution at* $t = 1$, *the green line is the solution at* $t = 2$, *and the red line the solution at* $t = 3$. *The dashed-lines are the corresponding exact solutions.*

Initial condition 3.6 Finally we study the case of moving cars on the right followed by an empty road in behind. The corresponding initial state is

$$\rho(x,0) = \begin{cases} 0, & x < 0, \\ 0.5, & x > 0. \end{cases} \tag{3.29}$$

We obtain a shock wave moving to the right with speed $s = 0.5$. From the numerical results, the empty road behind does not influence moving cars to the right. See Figure 3.6.

From these numerical solutions we can see the formation of shock waves and rarefaction waves. These solutions are only an approximation of real solutions. For instance, the

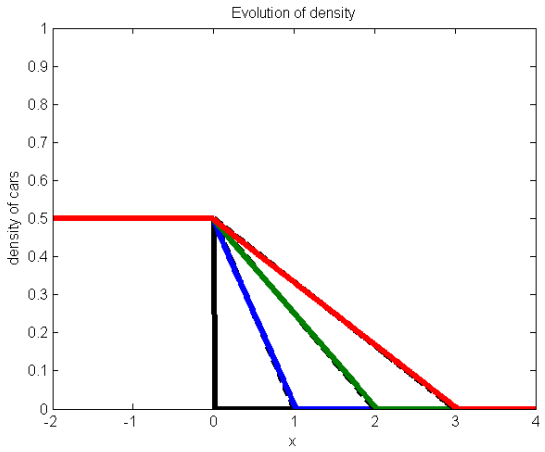

(a) Evolution of density

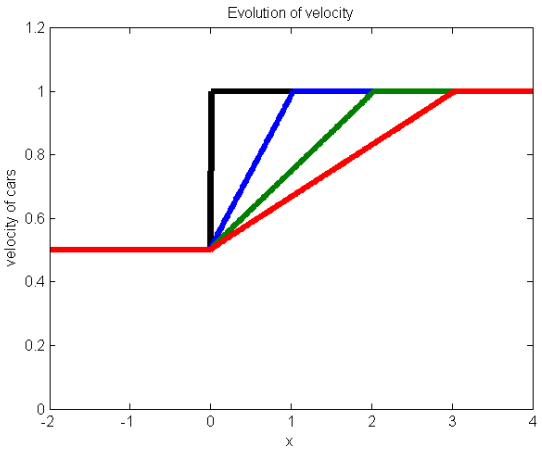

(b) Evolution of velocity

Figure 3.5: *Solution of the LWR model with data* $\rho_\ell = 0.5$ *and* $\rho_r = 0$. *Here the black solid line is the initial state, the blue line represents the solution at* $t = 1$, *the green line is the solution at* $t = 2$, *and the red line the solution at* $t = 3$. *The dashed-lines are the corresponding exact solutions.*

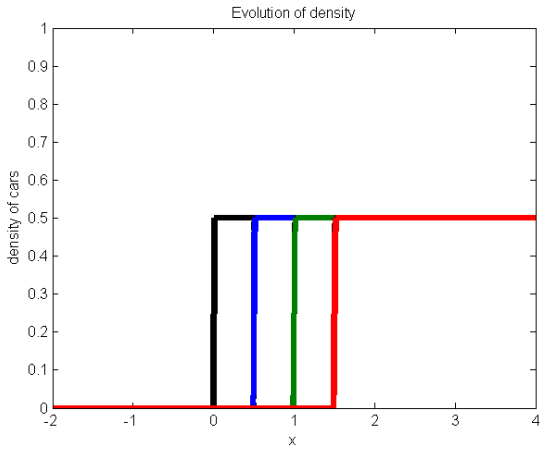

(a) Evolution of density

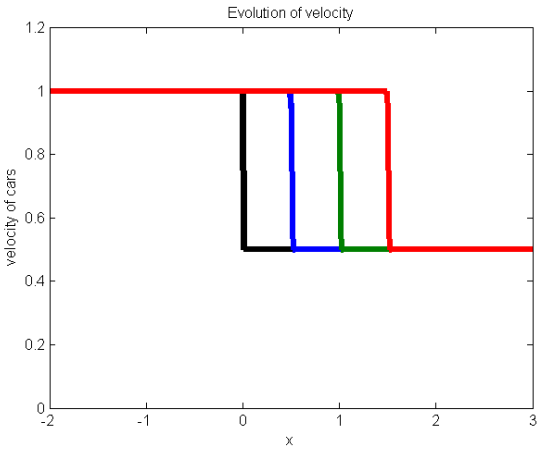

(b) Evolution of velocity

Figure 3.6: *Solution of the LWR model with data* $\rho_\ell = 0$ *and* $\rho_r = 0.5$. *Here the black solid line is the initial state, the blue line represents the solution at* $t = 1$, *the green line is the solution at* $t = 2$, *and the red line the solution at* $t = 3$. *The dashed-lines are the corresponding exact solutions.*

solutions after $t = 0$ are not exact jumps, while the theoretical solution to the LWR model with initial conditions (3.11) is still a jump at any time t. However, as $h \to 0$ and $k \to 0$ numerical solutions converge to the exact solutions.

(ii) Realistic Problem

Now we extend the above results by considering a highway in a range of 16×10^3 meters in spatial grig points with step size $\Delta x = 160$ meters and velocities are measured in m/s. In all numerical experiments performed in this sub-section the maximum density ρ_{max} is estimated to be $\rho_{max} = 1$. We consider different situations to investigate the effects of the

maximum velocity v_{max} on the behavior of the density profile. We want to simulate the traffic flow for a considered highway within six minutes.

- Let us fix $v_{max} = 20m/s$ and consider the initial densities as above, i.e., from (3.1) to (3.4). In this case the velocities in the previous case are scaled by a factor v_{max}. Numerical results are plotted in Figure 3.7.

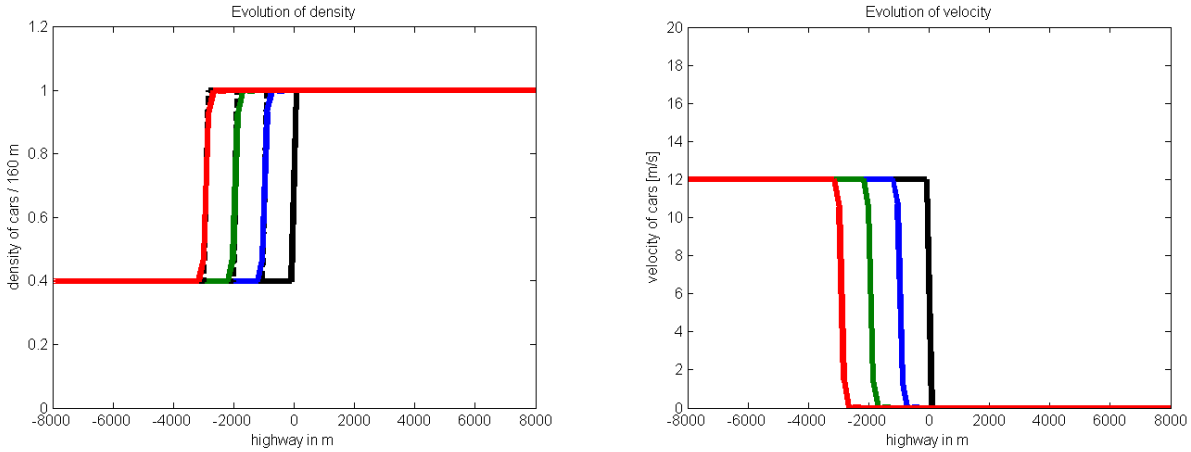

(a) Evolution of density

(b) Evolution of velocity

Figure 3.7: *Solution of the LWR model with data* $\rho_\ell = 0.4$ *and* $\rho_r = 1$, *and* $v_{max} = 20$. *Here the black solid line is the initial state, the blue line represents the solution at* 2 *minutes, the green line is the solution after* 4 *minutes, and the red line the solution after* 6 *minutes. The dashed-lines are the corresponding exact solutions.*

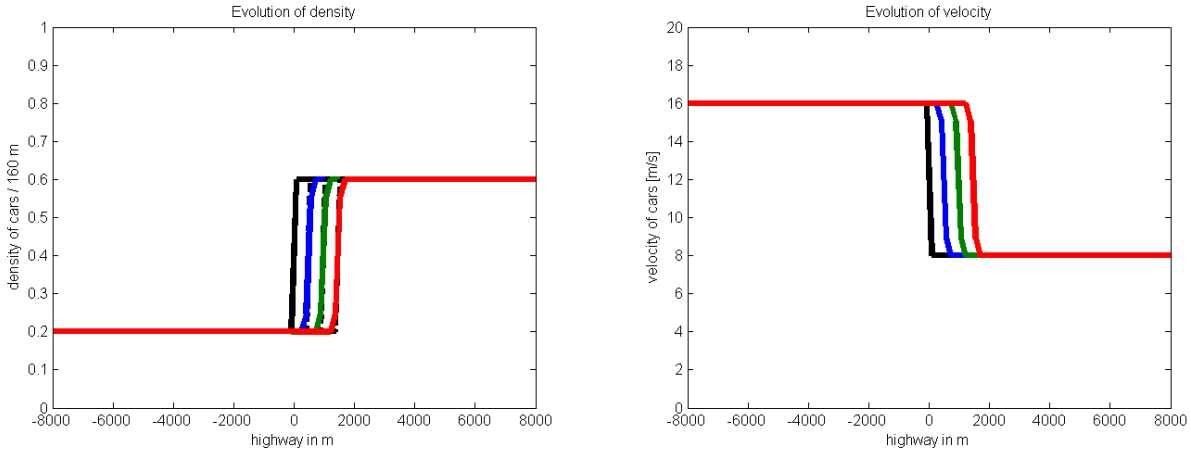

(a) Evolution of density

(b) Evolution of velocity

Figure 3.8: *Solution of the LWR model with data* $\rho_\ell = 0.2$ *and* $\rho_r = 0.6$, *and* $v_{max} = 20$. *Here the black solid line is the initial state, the blue line represents the solution at* 2 *minutes, the green line is the solution after* 4 *minutes, and the red line the solution after* 6 *minutes. The dashed-lines are the corresponding exact solutions.*

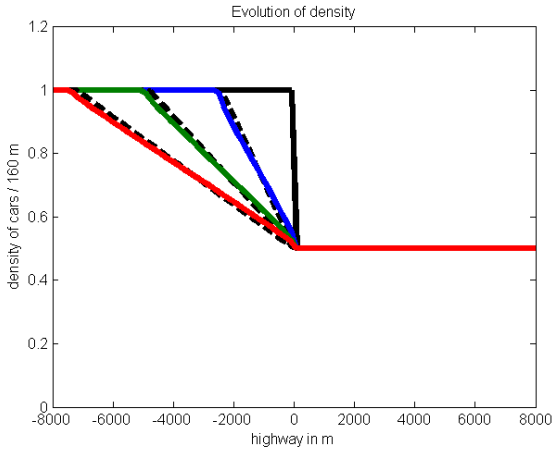

(a) Evolution of density

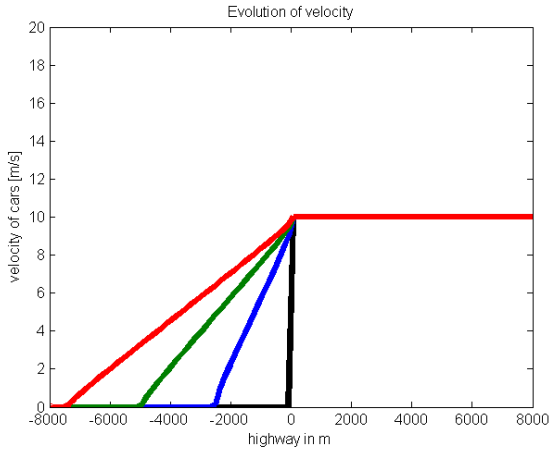

(b) Evolution of velocity

Figure 3.9: *Solution of the LWR model with data* $\rho_\ell = 1$ *and* $\rho_r = 0.5$, *and* $v_{max} = 20$. *Here the black solid line is the initial state, the blue line represents the solution at* 2 *minutes, the green line is the solution after* 4 *minutes, and the red line the solution after* 6 *minutes. The dashed-lines are the corresponding exact solutions.*

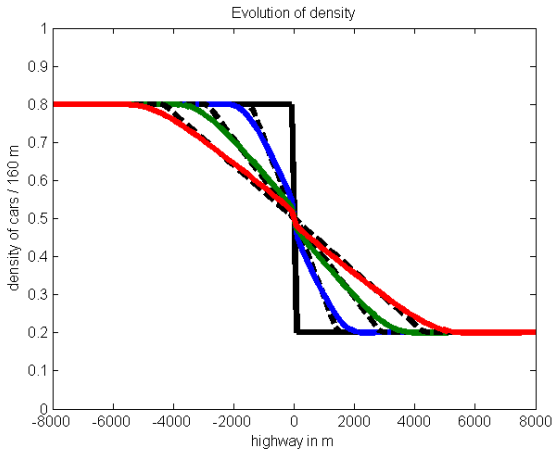

(a) Evolution of density

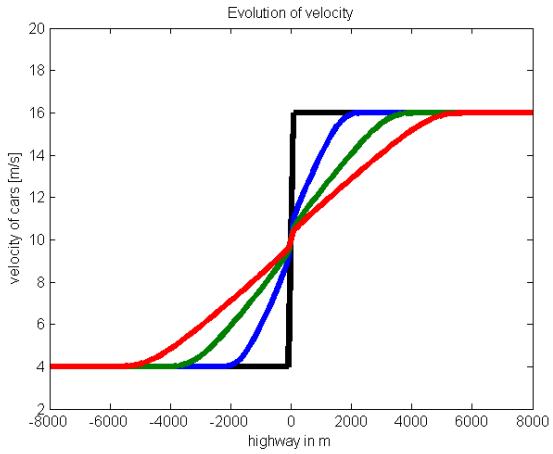

(b) Evolution of velocity

Figure 3.10: *Solution of the LWR model with data* $\rho_\ell = 0.8$ *and* $\rho_r = 0.2$, *and* $v_{max} = 20$. *Here the black solid line is the initial state, the blue line represents the solution at* 2 *minutes, the green line is the solution after* 4 *minutes, and the red line the solution after* 6 *minutes. The dashed-lines are the corresponding exact solutions.*

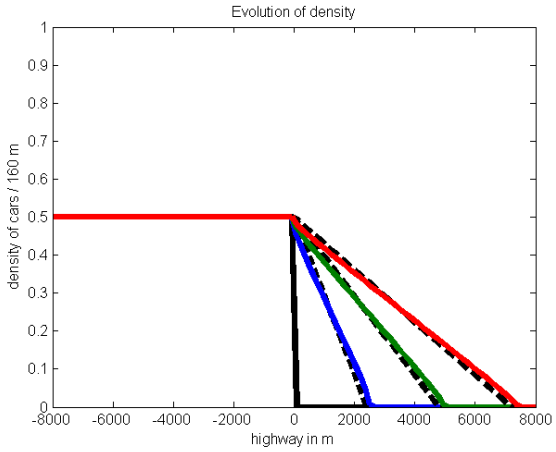

(a) Evolution of density

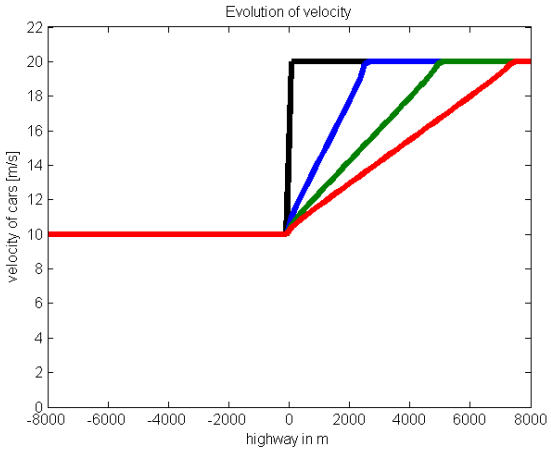

(b) Evolution of velocity

Figure 3.11: *Solution of the LWR model with data* $\rho_\ell = 0.5$ *and* $\rho_r = 0$, *and* $v_{max} = 20$. *Here the black solid line is the initial state, the blue line represents the solution at* 2 *minutes, the green line is the solution after* 4 *minutes, and the red line the solution after* 6 *minutes. The dashed-lines are the corresponding exact solutions.*

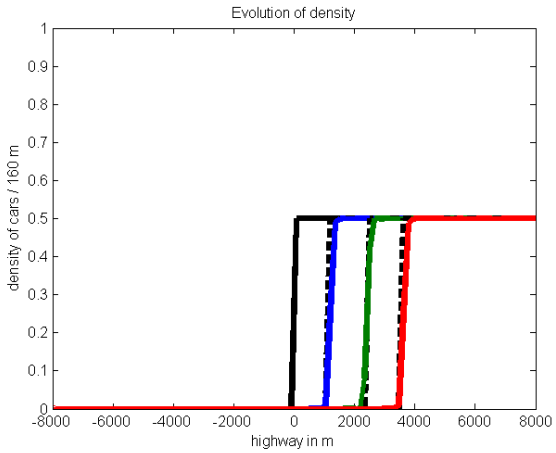

(a) Evolution of density

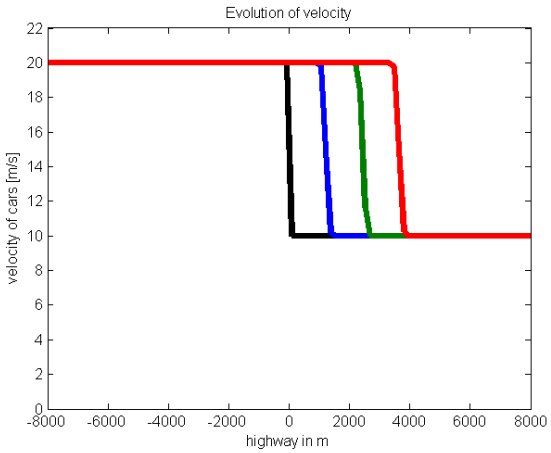

(b) Evolution of velocity

Figure 3.12: *Solution of the LWR model with data* $\rho_\ell = 0$ *and* $\rho_r = 0.5$, *and* $v_{max} = 20$. *Here the black solid line is the initial state, the blue line represents the solution at* 2 *minutes, the green line is the solution after* 4 *minutes, and the red line the solution after* 6 *minutes. The dashed-lines are the corresponding exact solutions.*

Chapter 4

Aw-Rascle Model of Traffic Flow

This chapter discusses the Aw and Rascle [2] (shortly Aw-Rascle) model, considered as an extension to the LWR model, in order to incorporate second-order effects. The Aw-Rascle model describes the traffic flow as a system of two partial differential equations describing evolutions of traffic density and momentum. From the literature, see e.g., [20], this model was designed to model the anisotropic traffic behavior, and incorporated the idea that the speed of each car does not change instantaneously and that drivers could look only ahead, determine the condition of the road in front of them and don't care about what happens behind.

The Aw-Rascle model is a purely nonlinear hyperbolic system of two conservation laws, hence a second-order model, in which no relaxation term is involved. We consider a well-posed initial value problem, which means, given the initial concentration of cars and velocity at any point x of the space, these two functions are defined for all future time $t \geq 0$ and any x, in a unique way and depend on the initial data. This means that, a small perturbation of the initial data produces only a small perturbation of the future solution.

4.1 Mathematical Model

The Aw-Rascle model is defined by the following system, (see [2] for more details):

$$\begin{aligned} \partial_t \rho + \partial_x(\rho v) &= 0, \\ \partial_t\Big(v + p(\rho)\Big) + v\partial_x\Big(v + p(\rho)\Big) &= 0. \end{aligned} \tag{4.1}$$

The first equation describes the conservation of mass, with ρ and v being, respectively, the density and the velocity of the car at point x and time t, whereas the second equation expresses the momentum equation, with a pressure law $p = p(\rho)$ considered as an increasing function of the density:

$$p = \rho^\gamma, \qquad \gamma > 0. \tag{4.2}$$

One may be interested on the behavior of this function p near the vacuum and the strict convexity of the function $\rho p(\rho)$. All our results in this work are valid under the following assumptions:

$$p \sim \rho^\gamma, \quad \text{near} \quad \rho = 0, \quad \gamma > 0, \quad \text{and} \quad \forall \rho, \rho p''(\rho) + 2p'(\rho) > 0. \tag{4.3}$$

Rewriting (4.1) under the form

$$\partial_t U + A(U)\partial_x U \quad = \quad 0,$$

where $U := (\rho, v)$, one can easily verify that the Jacobian matrix

$$A(U) \quad = \quad \begin{pmatrix} v & \rho \\ 0 & v - \rho p'(\rho) \end{pmatrix},$$

has real eigenvalues

$$\lambda_1 \; = \; v - \rho p' \quad \leq \quad \lambda_2 \; = \; v. \tag{4.4}$$

distinct except for $\rho = 0$ i.e., at vacuum. Therefore, the system (4.1) is strictly hyperbolic, except for $\rho = 0$, where the two eigenvalues are equal, and the matrix $A(U)$ is no longer diagonalizable. The corresponding eigenvectors are

$$R_1(U) \; = \; \begin{pmatrix} 1 \\ -p'(\rho) \end{pmatrix},$$

which corresponds to the eigenvalue $\lambda_1(U)$, and

$$R_2(U) \; = \; \begin{pmatrix} 1 \\ 0 \end{pmatrix},$$

corresponding to $\lambda_2(U)$. Due to the inequalities on the eigenvalues of the solution U (4.4) we observe that no wave travels faster than the speed of the vehicles v.

Definition 4.1.1 Let $\lambda_1 < \lambda_2 < ... < \lambda_n$ be n distinct real eigenvalues of the Jacobian matrix A. Since A depends on the solution U, so do the eigenvalues $\lambda_p, \quad p = 1, 2, ..., n$, and the corresponding eigenvectors r_p. Let ∇ denote the gradient with respect to U. Then an eigenvalue λ_p is called *genuinely nonlinear* [8], if the function

$$\nabla\lambda_p(U) \cdot r_p(U) \quad \neq \quad 0, \quad \text{for all values of} \quad U,$$

in other words if $\nabla\lambda_p(U)$ is not orthogonal to the corresponding eigenvector r_p. If on the other hand

$$\nabla\lambda_p(U) \cdot r_p(U) \quad \equiv \quad 0, \quad \text{for all values of} \quad U,$$

we call the $p - th$ characteristic field *linearly degenerate.*

For the system (4.1), we have

$$\begin{aligned} &\nabla\lambda_1(U) \cdot R_1(U) = -(2p' + \rho p'') \; \neq \; 0, \quad \text{by} \;\; (4.3), \\ &\nabla\lambda_2(U) \cdot R_2(U) \; \equiv \; 0, \quad \forall\, U. \end{aligned} \tag{4.5}$$

Therefore, the eigenvalue $\lambda_1(U)$ is *genuinely nonlinear*, whereas λ_2 is *linearly degenerate* (in the sense of (4.1.1).) Thus, depending on the data, the waves of the first family will be either shocks or rarefaction waves, while the waves of the second family will always be contact

discontinuities, i.e., waves whose propagation speed is always equal to the corresponding eigenvalue.

We know [2] that nonlinear hyperbolic systems admit discontinuous solutions that only make sense if the system is written in a *conservation law* [9, 10]. Hence, multiplying the first equation of system (4.1) by $v + p(\rho)$ and the second one by ρ yields

$$\begin{aligned} (v + p(\rho))\partial_t \rho + (v + p(\rho))\partial_x(\rho v) &= 0, \\ \rho\partial_t\Big(\rho(v + p)\Big) + \rho\partial_x\Big(\rho v(v + p)\Big) &= 0. \end{aligned}$$

Then adding the these two equations gives

$$\partial_t\Big(\rho(v + p)\Big) + \partial_x\Big(\rho v(v + p)\Big) = 0,$$

together with the mass equation we obtain the following conservative system:

$$\begin{aligned} \partial_t \rho + \partial_x(\rho v) &= 0, \\ \partial_t\Big(\rho(v + p)\Big) + \partial_x\Big(\rho v(v + p)\Big) &= 0. \end{aligned} \tag{4.6}$$

This is equivalent to the non-conservative system (4.1). With the choice of the pressure function (4.2) the model satisfies the following five principles [2]:

- Principle A: the system (4.6) must be hyperbolic.
- Principle B: when solving the Riemann problem associated with (4.6) and a given arbitrary bounded nonnegative Riemann data in a convex invariant region Ω, (will be defined later) of the plane, the density and the velocity must remain nonnegative and bounded from above all time.
- Principle C: in solving the same Riemann problem with arbitrary data $U_0 = (U_\ell, U_r)$, all waves connecting any state $U = (\rho, v)$ behind it must have a propagation speed (shock speed or eigenvalue) *at most* equal to the velocity v of the cars.
- Principle D: the solution to the Riemann problem must agree with the qualitative properties that each driver observes every day in practice. Braking produces shock waves, whose propagation speed can be either negative or positive, whereas accelerating produces rarefaction waves which in any case satisfy Principle C above.
- Principle E: near the vacuum, the solution to the Riemann problem must be very sensitive to the data, i.e., there must be no continuous dependence with respect to the initial data at $\rho = 0$.

4.2 The Riemann Problem of the Aw-Rasle Model

Now let us introduce a new conservative variable

$$y := \rho v + \rho p(\rho). \tag{4.7}$$

With this, system (4.6) can be rewritten in the following form

$$\begin{aligned} \partial_t \rho + \partial_x(\rho v) &= 0, \\ \partial_t y + \partial_x(y v) &= 0. \end{aligned} \tag{4.8}$$

This can be rewritten in the matrix form, by setting $U := (\rho, y)$, as follows

$$U_t + f(U)_x = 0,$$

with flux function $f(U) = (\rho v, y v)$.

We want to solve the Riemann problem [1, 9, 10] of the Aw-Rascle model associated with the system (4.8) and with the following piecewise initial condition having a single discontinuity around the space coordinate $x = 0$

$$U(x,0) = \begin{cases} U_\ell, & \text{if } x < 0, \\ U_r, & \text{if } x > 0. \end{cases} \tag{4.9}$$

In our notations, the initial state components are $U_\ell = (\rho_\ell, y_\ell)$, and $U_r = (\rho_r, y_r)$. According to [7], the Riemann problem is solved by a combination of two families of waves: 1-waves corresponding to the first eigenvalue λ_1 and 2-waves corresponding to λ_2.

4.2.1 Wave Solutions of the Riemann Problem of the Aw-Rascle Model

We now turn to the study of piecewise continuous solutions of (4.8) associated with (4.9). Each of the 2 conservation laws must satisfy the Rankine-Hugoniot jump condition [10]. We now have

$$s[U_k] = [f_k], \quad k = 1, 2, \tag{4.10}$$

must hold across every discontinuity, where $[g] := g_r - g_l$ denote the jump of any quantity g through the discontinuity, and s is the propagation speed of the discontinuity. In the above late notation, index k specifies the component of U and f, and condition (4.10) must hold for each component. Next we formulate an entropy condition for the defined Riemann problem that requires all characteristics on either side of a discontinuity to run into the line of discontinuity, which is the case if the characteristic speed on the left is greater, on the right less, than s [7, 8, 10]. This gives the mathematical inequalities

$$\lambda(U_\ell) > s > \lambda(U_r).$$

For the k^{th} field we require that for some index $k = 1, 2$ in our case study,

$$\begin{aligned} \lambda_k(U_\ell) > s > \lambda_k(U_r), \\ \lambda_{k-1}(U_\ell) < s < \lambda_{k+1}(U_r). \end{aligned} \tag{4.11}$$

Definition 4.2.1 Waves with wave speed λ_k are called *k-waves.* A discontinuity across which (4.10) and (4.11) are satisfied is called a *k-shock.*

In the following section, we describe 1-shock waves i.e., those waves where U_r and U_ℓ differ little; it is understood that U_ℓ is to the left of U_r, and 1-rarefaction waves as well as 2-contact discontinuity, by giving their analytical expressions.

Elementary Wave Solutions of the Riemann Problem

In order to solve the Riemann problem, we first need to compute the Riemann invariants in the sense of Lax [8] associated with each eigenvalue λ_k, $k = 1, 2$.

Definition 4.2.2 *[8]*
A scalar function w of U is called a *1-Riemann invariant in the sense of Lax* if

$$\nabla w \cdot r_1 \quad \equiv \quad 0, \tag{4.12}$$

and we call $z = z(U)$ a 2-Riemann invariant in the sense of Lax if

$$\nabla z \cdot r_2 \quad \equiv \quad 0. \tag{4.13}$$

Now using the expressions of r_1 and r_2 here we obtain

$$\begin{aligned} w(U) &= v + p(\rho), \\ z(U) &= v. \end{aligned} \tag{4.14}$$

According to the genuinely nonlinearity of the eigenvalue $\lambda_1(U)$, the Riemann problem may have 1-shock and 1-rarefaction waves. These are called waves of the first family, in order words, waves with speed $\lambda_1(U)$.

(a) ***1-shock waves*:**

From (4.11), the 1-shock waves satisfy the following Lax entropy condition:

$$\lambda_1(U_r) < s < \lambda_1(U_\ell), \quad s < \lambda_2(U_r), \tag{4.15}$$

where the shock wave speed s is determined by the Rankine-Hugoniot jump condition (4.10).

$$\begin{aligned} s[\rho] &= [\rho v], \\ s[y] &= [yv], \end{aligned} \tag{4.16}$$

which is a system of two equations with three unknowns: ρ, y and s. In order to solve this system we will have to express s and y in terms of the density ρ. Solving for s from these two equations yields

$$\frac{[\rho v]}{[\rho]} \quad = \quad s \quad = \quad \frac{[yv]}{[y]},$$

equivalent to

$$\frac{\rho_r v_r - \rho_\ell v_l}{\rho_r - \rho_\ell} \quad = \quad \frac{y_r v_r - y_\ell v_\ell}{y_r - y_\ell}.$$

This gives

$$y_\ell \rho_r v_r + y_r \rho_\ell v_\ell \quad = \quad y_r \rho_\ell v_r + y_\ell \rho_r v_\ell$$

Rearranging the terms and dividing each by $\rho_r\rho_\ell$ gives

$$\Big(\frac{y_\ell}{\rho_\ell} - \frac{y_r}{\rho_r}\Big)(v_r - v_\ell) \quad = \quad 0.$$

Therefore, there are two cases to be considered:

(i) if $v_r - v_\ell \neq 0$, then

$$\frac{y_r}{\rho_r} \quad = \quad \frac{y_\ell}{\rho_\ell},$$

From (4.7) this is equivalent to

$$v_r + \rho_r^\gamma \quad = \quad v_\ell + \rho_\ell^\gamma,$$

or by (4.14)

$$w(U_r) \quad = \quad w(U_\ell).$$

This determines the curve of a 1-shock wave connecting the states U_ℓ, given on the left side of the discontinuity, to the state U_r on the right side.

In general, a given state U_ℓ to the left can be connected to any other state U to the right by a 1-shock wave if and only if

$$w(U) \quad = \quad w(U_\ell) \tag{4.17}$$

with $w(U)$ already defined in (4.14). This is equivalent to

$$v + \rho^\gamma \quad = \quad v_\ell + \rho_\ell^\gamma. \tag{4.18}$$

(ii) if $v_r - v_\ell = 0$, then

$$v_r = v_l. \tag{4.19}$$

This case corresponds to a contact discontinuity of the second family.

(a) Rarefaction Waves

The Riemann problem of our model has the property that the solution U is constant along all rays of the form $x = \beta t$. From this we have a new variable $\beta = x/t$. As a consequence, the solution is a function of x/t alone, and is called a *similarity solution* of the PDE. Therefore, the solution $u(x,t)$ is only a function of β. Let us note this using $u(x,t) = w(\beta)$ which gives after substitution into the equation (give reference of the equation here)

$$\Big(f'(w) - \beta\Big)w' \quad = \quad 0, \tag{4.20}$$

with $w = w(\beta)$. One possible solution of (4.20) is $w' = 0$, which gives w is constant. Any constant function is a similarity solution of the conservation law, and indeed the

rarefaction wave takes this form for $\beta < \beta_1$, and $\beta < \beta_2$, for some constants β_1 and β_2 being specified later. One may think of what happens in between. For $\beta_1 < \beta < \beta_2$, the function w is smoothly varying and $w' \neq 0$. Note that (4.20) can also be written in an eigenvalue problem as follows:

$$f'(w)w' = \beta w', \tag{4.21}$$

which says that w' is proportional to some eigenvector $r_p(w)$ of $f'(w)$. This implies

$$w' = \alpha(\beta) r_p(w), \tag{4.22}$$

where $\alpha(\beta)$ is a proportionality factor. Hence the values w all lie along some integral curve of r_p [9]. In particular, the states $u_\ell = w(\beta_1)$ and $u_r = w(\beta_2)$ both lie on the same integral curve. This is a necessary condition for the existence of a rarefaction wave connecting states $u\ell$ to u_r, but this is not sufficient. We also need $\beta = x/t$ to be monotonically increasing as $w(\beta)$ moves from u_ℓ to u_r, along the integral curve in order to have a single-valued rarefaction wave. Form (4.21) we see that β is an eigenvalue of $f'(w)$, that is,

$$\beta = \lambda_p(w). \tag{4.23}$$

This implies that w is constant along the ray $x = \lambda_p(w)t$, and hence each constant value of w propagates with speed $\lambda_p(w)$. By (4.23), monotonicity of η simply implies monotonicity of $\lambda_p(w)$ as w moves from u_ℓ to u_r. From a given state u_ℓ we can move to another state u_r along the integral curve only in the direction in which λ_p is increasing. If λ_p has a local maximum at u_ℓ, then there is no rarefaction waves with this left state [9]. Now let us explicitly determine the function $w(\beta)$. To do this, we first need to determine the scalar factor $\alpha(\beta)$ appearing in (4.22) by differentiating

A given state U_ℓ to the left can be connected to any state U to the right by a 1-rarefaction wave if and only if

$$\begin{aligned} \frac{y}{\rho} &= \frac{y_\ell}{\rho_\ell}, \\ \lambda_1(U) &= \beta. \end{aligned}$$

which is equivalent to

$$\begin{aligned} v + \rho^\gamma &= v_\ell + \rho_\ell^\gamma, \\ v - \gamma\rho^\gamma &= \beta. \end{aligned} \tag{4.24}$$

4.2.2 Analytical Solutions and Examples

We briefly discuss the 5 general cases of the Riemann data we should consider for the Rascle model. Note that all these cases can also be found in [2]. As a remainder, we mostly use the notations $U_\ell = (\rho_\ell, y_\ell)$ to represent the left state, $U_m = (\rho_m, y_m)$ is the intermediate state, and $U_r = (\rho_r, y_r)$ stands for the right state. The goal of this section is to first connect the

given left state U_ℓ to a determined middle state U_m by a wave of the first family and then connect this intermediate state U_m to the right state U_r by a contact discontinuity of the second family. Equivalently, one may also go the other way around, to start from U_r and to arrive at U_ℓ. In any of these cases, the 1-wave is a rarefaction wave if $\rho_m < \rho_\ell$ or is a Lax shock wave in the opposite case, except if the vacuum state (i.e. if $\rho = 0$) is involved, since at the vacuum the two eigenvalues are equal, thus some of the inequalities in (4.15) become equalities.

Case 1: $\rho_\ell > 0, \quad \rho_r > 0, \quad 0 \le v_r \le v_\ell$:

In this case we have a unique solution $U(x,t)$ that consists of a 1-shock wave connecting the state U_ℓ given to the left to the intermediate state U_m followed by a 2-contact discontinuity connecting U_m to the state U_r on the right. Here the 1-shock must satisfy the shock curve defined in (4.18) and the contact discontinuity satisfies (4.19). The goal here is to solve for the intermediate state U_m which satisfies the following two equations simultaneously:

$$\begin{aligned} v_m + \rho_m^\gamma &= v_\ell + \rho_\ell^\gamma, \\ v_m &= v_r, \end{aligned}$$

which gives

$$\begin{aligned} \rho_m &= (v_\ell - v_r + \rho_\ell^\gamma)^{1/\gamma}, \\ v_m &= v_r. \end{aligned} \tag{4.25}$$

Thus the solution $U(x,t)$ takes the form

$$U(x,t) = \begin{cases} U_\ell, & \beta \le s, \\ U_m, & s < \beta \le v_r, \\ U_r, & \beta > v_r, \end{cases} \tag{4.26}$$

with $\beta = x/t$ and s the shock speed computed from the Rankine-Hugoniot condition (4.10)

$$s = \frac{\rho_m v_m - \rho_\ell v_\ell}{\rho_m - \rho_\ell}. \tag{4.27}$$

Case 2: $\rho_\ell > 0, \quad \rho_r > 0, \quad v_\ell \le v_r \le v_\ell + \rho_\ell^\gamma$

Here the solution $U(x,t)$ consists of a 1-rarefaction wave connecting the state U_ℓ given to the left to the intermediate state U_m followed by a 2-contact discontinuity connecting U_m to the state U_r on the right, where the 1-rarefaction wave satisfies the rarefaction curve (4.24). Therefore the solution is defined by

$$U(x,t) = \begin{cases} U_\ell, & \beta \le \lambda_1(U_\ell), \\ U^*, & \lambda_1(U_\ell) < \beta \le \lambda_1(U_m), \\ U_m, & \lambda_1(U_m) < \beta \le v_r, \\ U_r, & \beta > v_r, \end{cases} \tag{4.28}$$

where ρ_m and v_m are given by (4.25), and ρ^*, y^* solves (4.24), that is,

$$\begin{aligned} v^* + \rho^{*\gamma} &= v_\ell + \rho_\ell^\gamma, \\ v^* - \gamma\rho^{*\gamma} &= \beta. \end{aligned} \tag{4.29}$$

This gives

$$\begin{aligned} \rho^* &= \Big(\frac{1}{\gamma+1}(v_\ell + \rho_\ell^\gamma - \beta)\Big)^{1/\gamma}, \\ v^* &= \frac{1}{\gamma+1}\Big(\beta + \gamma(v_\ell + \rho_\ell^\gamma)\Big), \end{aligned} \tag{4.30}$$

Case 3: $\rho_\ell > 0, \quad \rho_r > 0, \quad v_\ell + \rho_\ell^\gamma < v_r$

In this case the intermediate state is the vacuum wave with vacuum states let us say U_1 and U_2. Thus the solution $U(x,t)$ consists of a 1-shock wave connecting the left state U_ℓ to U_m followed by a vacuum wave which connect U_1 and U_2, followed by a 2-contact discontinuity connecting U_2 to the state U_r on the right. Again the 1-shock must satisfy (4.18) and the contact discontinuity satisfies (4.19).

$$U(x,t) = \begin{cases} U_\ell, & x \le \lambda_1(U_\ell)t, \\ U^*, & \lambda_1(U_\ell)t < x \le \lambda_1(U_1)t, \\ U_m, & \lambda_1(U_1)t < x \le \lambda_2(U_2)t, \\ U_r, & x > \lambda_2(U_2)t, \end{cases}$$

In contrast to Case 2, here the intermediate state $U_m = (0,0)$. The rarefaction state $U^* = (\rho^*, y^*)$ is already defined in (4.30) above. The vacuum state U_1 is the intersection of the curve $w(U) = w(U_\ell)$ with the axis $\rho = 0$, this gives $v_1 = v_\ell + \rho_\ell^\gamma$. The state U_2 is the point of coordinates $\rho_2 = 0, v_2 = v_r$. In other words, $U_1 = (0, v_\ell + \rho_\ell^\gamma)$ and $U_2 = (0, v_r)$.

This gives

$$U(x,t) = \begin{cases} U_\ell, & x \le (v_\ell - \gamma\rho_\ell^\gamma)t, \\ U^*, & (v_\ell - \gamma\rho_\ell^\gamma)t < x \le (v_\ell + \rho_\ell^\gamma)t, \\ U_m, & (v_\ell + \rho_\ell^\gamma)t < x \le v_r t, \\ U_r, & x > v_r t, \end{cases} \tag{4.31}$$

Case 4: $\rho_\ell > 0, \quad \rho_r = 0$

In this case we connect the Riemann datum U_ℓ on the left to the origin $U_r = (0,0)$, on the right. This case is similar to Case 3, but now there is no need to add a contact discontinuity since the state on the right is the origin, which is on the rarefaction curve issued from the left state. Therefore, the solution $U(x,t)$ is only a 1-rarefaction wave given by

$$U(x,t) = \begin{cases} U_\ell, & x \le (v_\ell - \gamma\rho_\ell^\gamma)t, \\ U^*, & (v_\ell - \gamma\rho_\ell^\gamma)t < x \le (v_\ell + \rho_\ell^\gamma)t, \\ U_r, & x >\le (v_\ell + \rho_\ell^\gamma)t, \end{cases} \tag{4.32}$$

with $U_r = (0,0)$.

Case 5: $\rho_\ell = 0, \quad \rho_r > 0$

Here the Riemann datum U_r on the right will be connected to the vacuum state on the left by a 2-contact discontinuity. This case is similar to Case 1, but now the wave of first family has disappeared.

The solution $U(x,t)$ is given by a single contact discontinuity moving at the speed of the leading cars and takes the following form

$$U(x,t) = \begin{cases} U_\ell, & x \le v_r t, \\ U_r, & x > v_r t, \end{cases} \tag{4.33}$$

but $U_\ell = (0,0)$, and the shock speed $s = v_r$.

4.3 Numerical Implementation of the Godunov Method

We now discuss how to get a stable, convergent and efficient numerical method. In a linear hyperbolic system, Godunovs method is stable and convergent if the Courant-Friedrichs-Lewy (CFL) number is less than unity. Similarly we require the CFL number be less than unity for Aw-Rascle model. In all our numerics we use

$$\frac{k}{h}\Big(\max\Big|\lambda_i(U_j^n)\Big|\Big) = 0.99, \quad i = 1,2 \tag{4.34}$$

where the maximum is taken over all $j = 1, ..., N_x$ in order to get the maximum wave velocity throughout the domain at time t^n. In the Aw-Rascle model we have

$$\begin{aligned} \lambda_1(U_j^n) &= v_j^n - \gamma \rho_j^n, \\ \lambda_2(U_j^n) &= v_j^n. \end{aligned}$$

The solution to the Riemann problem is important both theoretically and computationally. One can compute the numerical solutions when all Riemann problems are well-posed and solvable at each step of the iteration. However, when the left and right states for a Riemann problem are far from each other, the intermediate state U_m for the wave solutions may be out of the domain of validity, e.g., $\rho_m < 0$. In this case, we have a vacuum problem and hence the numerical solutions cannot be uniquely determined. The cost of solving the Riemann problem determines the computational efficiency of the numerical method. Like in the LWR model, we also use the Godunov method to numerically simulate the Aw-Rascle model.

4.3.1 The Godunov Method

In contrary to the LWR model, the Aw-Rascle model is a system of two equation and its flux function

$$f(U) = \begin{bmatrix} \rho v \\ y v \end{bmatrix} \tag{4.35}$$

is a vector of two components. Hence its corresponding numerical Godunov flux is also a vector of two components, let us say

$$F_G(U) \;=\; \begin{bmatrix} H(U) \\ G(U) \end{bmatrix}$$

Here the first component H is associated with the flux of the first conservative variable ρ, and the second component G corresponds to the second variable y. Define the control volumes or cells V_j as follows

$$V_j = \;\Big[x_{j-\frac{1}{2}}, x_{j+\frac{1}{2}}\Big), \qquad x_{j+1/2} \;=\; x_j + \frac{h}{2}, \qquad j \;=\; 0, \pm 1, \pm 2, ...$$

Let $\bar{U}(x,t)$ be the solution of the following Riemann problem

$$\bar{U}_t + f(\bar{U})_x \;\;=\;\; 0,$$

where f is defined by (4.35) above. Associate this problem with the following initial value

$$\bar{U}(x,t^n) = \;\begin{cases} U_j^n, & x < x_{j+\frac{1}{2}}, \\ U_{j+1}^n, & x > x_{j+\frac{1}{2}}. \end{cases}$$

The solution of this Riemann problem is a similarity of the form

$$\bar{U}(x,t) \;\;=\;\; U_R\Big(\beta; U_j^n, U_{j+1}^n\Big), \qquad \beta \;=\; \frac{x - x_{j+\frac{1}{2}}}{t - t^n}.$$

Clearly, $\beta = 0$ for $x = x_{j+\frac{1}{2}}$, hence the numerical flux is defined by

$$F_G\Big(U_j^n, U_{j+1}^n\Big) \;\;=\;\; f\Big(U_R\Big(0; U_j^n, U_{j+1}^n\Big)\Big). \tag{4.36}$$

Defining the numerical flux components

$$\begin{array}{rclcrcl} H_j^n & = & H(\rho_j^n, \rho_{j+1}^n), & & H_{j-1}^n & = & H(\rho_{j-1}^n, \rho_j^n), \\ G_j^n & = & G(y_j^n, y_{j+1}^n), & & G_{j-1}^n & = & G(y_{j-1}^n, y_j^n) \end{array}$$

then the Godunov scheme applied to solve the Rascle model is solving the following finite differences equations simultaneously:

$$\begin{array}{rcl} \rho_j^{n+1} = & \rho_j^n - \dfrac{k}{h}\Big(H_j^n - H_{j-1}^n\Big), \\ y_j^{n+1} = & y_j^n - \dfrac{k}{h}\Big(G_j^n - G_{j-1}^n\Big), \end{array} \tag{4.37}$$

Remember that here h stands for the grid mesh size and k represents the time step size.

4.3.2 Numerical Examples

We now present our numerical results for the Aw-Rascle model. We first consider a simple case of the Aw-Rascle model, in which parameters ρ_{max} and v_{max} are chosen to be unit. Then after we extend our results from this simple case to a realistic case where parameters in the model are chosen to be realistic data; here we consider the highway to be measured in meters and velocity in m/s. In all cases we study different Riemann problems and present the results for two different choices of γ : we propose $\gamma = 1$ and $\gamma = 2$. As an exercise we checked the performance of the proposed numerical scheme by performing various numerical tests with two different mesh sizes: $\Delta x = 0.01$ and $\Delta x = 0.002$. Note that only numerical results for $\Delta x = 0.01$ are presented in this thesis.

(i) Simple case

In this simple case we fix $v_{max} = 1$. We prefer to describe the legend of the plots presented in this case as follows: the black solid line represents the initial state of the Rascle model, the blue solid line is the density profile at $t = 2$, the green solid line is the density profile at $t = 4$, the red solid line represents the density at $t = 6$, the dashed-line represents the exact density at $t = 2$, the dotted-line is the exact density at $t = 4$, and finally the exact density at $t = 6$ is manifested by the dashed-dotted line. For our study we propose different Riemann problems presented here below.

Initial condition 4.1 Now consider the following initial state:

$$\rho(x,0) = \begin{cases} 0.5, & x < 0, \\ 0.8, & x > 0, \end{cases} \qquad v(x,0) = \begin{cases} 0.6, & x < 0, \\ 0.4, & x > 0. \end{cases} \tag{4.38}$$

Since $v_r < v_\ell$, then the exact solution of this Riemann problem is a shock wave described in (4.33) traveling with negative speed, i.e., the wave moves to the left, followed by a contact discontinuity moving to the right with the speed of the leading cars $v_r = 0.4$. Both numerical and exact results are plotted at different proposed times in Figure 4.1.

From these results we observe a small change in the density profile which results in change of velocity profile. With $\gamma = 1$ the shock moves to the left at speed $s = 0.10$ and intermediate state in this case is $\rho_m = 0.7$. This slightly decreases to $\rho_m = 0.67$ for $\gamma = 2$, and the shock speed is increased to $s = 0.185$, still moving to the left.

Initial condition 4.2 Consider the following Riemann data

$$\rho(x,0) = \begin{cases} 0.8, & x < 0, \\ 0.6, & x > 0, \end{cases} \qquad v(x,0) = \begin{cases} 0.6, & x < 0, \\ 1, & x > 0. \end{cases} \tag{4.39}$$

In Figure 4.2 we present both exact and numerical solutions of this Riemann problem. The exact solution is a rarefaction wave followed by a contact discontinuity moving to the right with the chosen maximum speed $v_r = 1$, and the corresponding numerical solutions are plotted at different times. We observe from these results that the contact discontinuity is well approximated by the Godunov scheme proposed in this thesis.

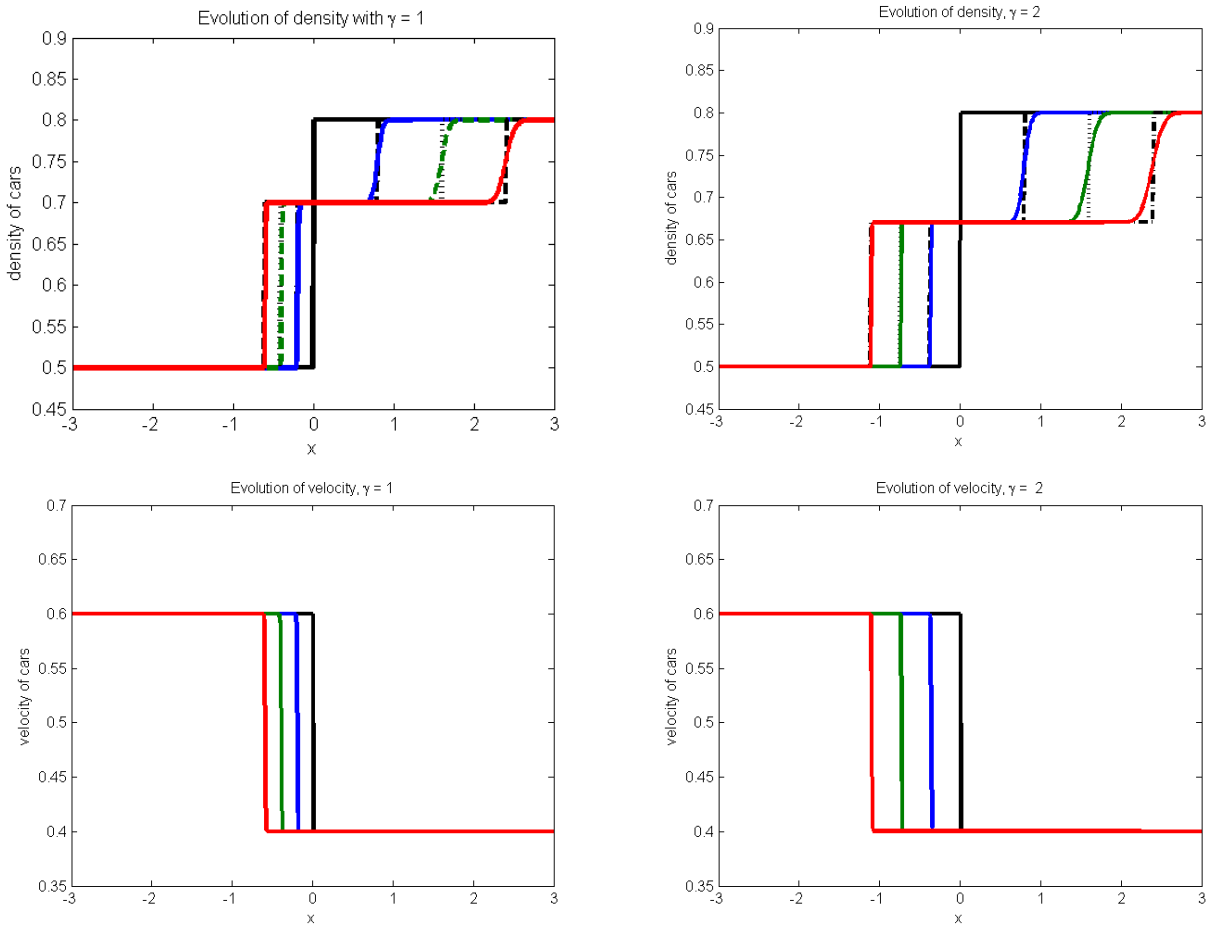

Figure 4.1: *Solution of the Rascle model with Riemann data* $\rho_\ell = 0.5$, $v_\ell = 0.6$, $\rho_r = 0.8$, $v_r = 0.4$. *On the top from left to right, density profiles with* $\gamma = 1$ *and* $\gamma = 2$, *respectively, are plotted and their corresponding velocity profiles at the bottom.*

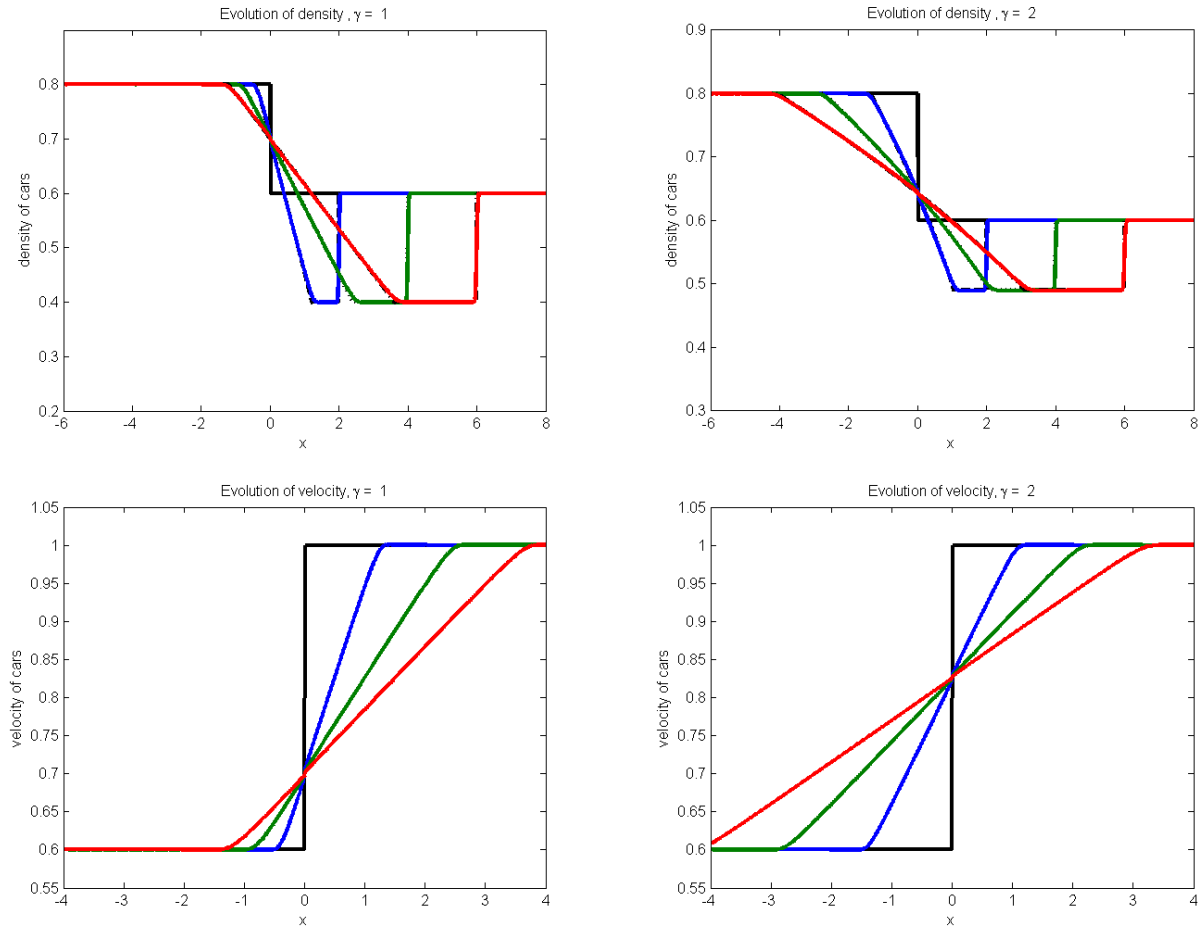

Figure 4.2: *Solution of the Rascle model with Riemann data* $\rho_\ell = 0.8,\ v_\ell = 0.6,\ \rho_r = 0.6,\ v_r = 1$. *On the top from left to right, density profiles with* $\gamma = 1$ *and* $\gamma = 2$, *respectively, are plotted and their corresponding velocity profiles at the bottom.*

Initial condition 4.3 Here the case of faster cars on the right followed by slower ones in behind is considered. The corresponding data are

$$\rho(x,0) \;=\; \begin{cases} 0.4, & x<0, \\ 0.1, & x>0, \end{cases} \qquad v(x,0) \;=\; \begin{cases} 0.1, & x<0, \\ 0.9, & x>0. \end{cases} \tag{4.40}$$

The exact solution of the Rascle model is now given by a rarefaction wave connected to a vacuum state, which followed by a contact discontinuity going to the right. For this problem our numerical scheme fails to capture the fake wave that connects the rarefaction wave to the vacuum state. Corresponding results are plotted in Figure 4.3. From this we can see the generation of an artificial jump and this cannot be reduced even if the mesh size is reduced.

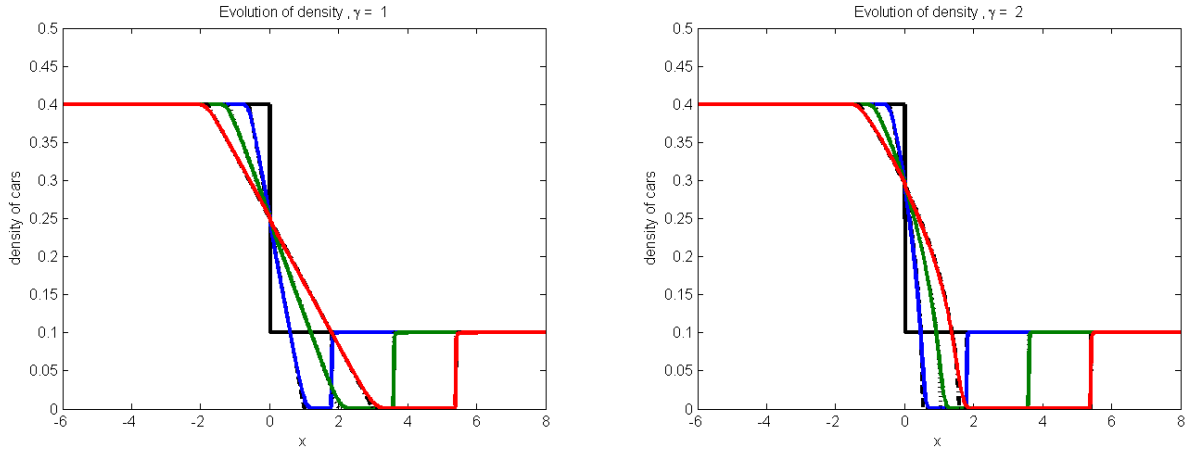

(a) with $\gamma = 1$ (b) with $\gamma = 2$

Figure 4.3: *Density profiles of the Rascle model with Riemann data* $\rho_\ell = 0.4,\ v_\ell = 0.1,\ \rho_r = 0.1,\ v_r = 0.9$.

Note that in this situation, from (4.7) the velocity is not defined due to vacuum wave that generate an artificial jump in density. For this reason we skip the velocity profiles in Figure 4.3.

Initial condition 4.4 The situation of faster cars on the right followed by slower ones in behind is considered. The corresponding data are

$$\rho(x,0) \;=\; \begin{cases} 0.5, & x<0, \\ 0, & x>0, \end{cases} \qquad v(x,0) \;=\; \begin{cases} 0.6, & x<0, \\ 1, & x>0. \end{cases} \tag{4.41}$$

The exact solution in this case is a single rarefaction wave going to the right. In Figure 4.4, both exact and numerical solutions at different times are plotted.

Here we observe that the empty road on the right does not affect drivers from the left and with $\gamma = 2$, the exact density profile is well approximated by the numerical solution.

Initial condition 4.5 We now turn to the case of moving cars on the right followed by an empty road in behind. The corresponding data are

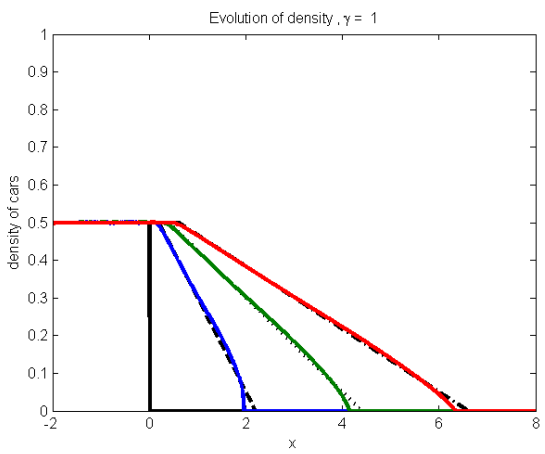

(a) with $\gamma = 1$

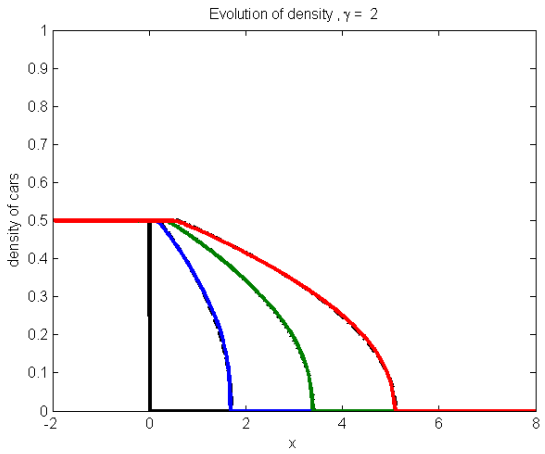

(b) with $\gamma = 2$

Figure 4.4: *Density profiles of the Rascle model with the Riemann data* $\rho_\ell = 0.5, \quad v_\ell = 0.6,$ $\rho_r = 0, \quad$ *and* $v_r = 1.$

$$\rho(x,0) = \begin{cases} 0, & x < 0, \\ 0.5, & x > 0, \end{cases} \qquad v(x,0) = \begin{cases} 0.5, & x < 0, \\ 0.5, & x > 0. \end{cases} \tag{4.42}$$

In this case we have, for the Rascle model, a single right-going contact discontinuity with speed of the leading cars $v_r = 1$. The corresponding results are plotted in Figure 4.5. From these results one can see that the numerical solution at any fixed time properly approximates the exact contact discontinuity. In this case moving cars on the right are not influenced by the free space behind them.

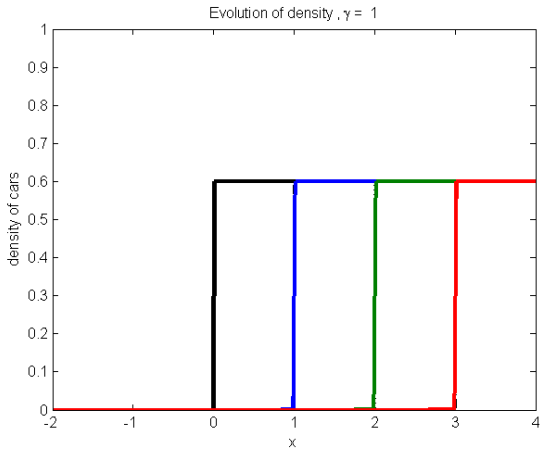

(a) with $\gamma = 1$

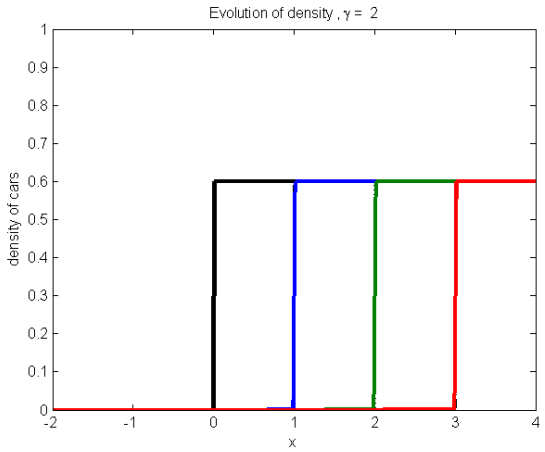

(b) with $\gamma = 2$

Figure 4.5: *Density profiles of the Rascle model with the Riemann data* $\rho_\ell = 0, \quad v_\ell = 0.5,$ $\rho_r = 0.5, \quad$ *and* $v_r = 0.5.$

(ii) Realistic problem

We extend the above results by choosing $v_{max} = 20m/s$ and considering a highway in a range of 16×10^3 meters in spatial grig points with step size $\Delta x = 160$ meters. All velocities

in this case are measured in m/s. For the legend of the plots presented here, the black solid line represents the initial state of the Rascle model, the blue solid line is the density profile after 2 minutes, the green solid line is the density profile at 4 minutes, the red solid line represents the density at 6 minutes, the dashed-line represents the exact density profile at 2 minutes, the dotted-line is the exact density after 4 minutes and finally the exact density at 6 minutes is manifested by the dashed-dotted line. In all numerical experiments performed here the maximum density ρ_{max} is estimated to be $\rho_{max} = 1$ like in the previous case. We want to simulate the traffic flow for a considered highway within six minutes. We consider different situations to investigate the effects of parameters appeared in the model, such as γ and the maximum velocity v_{max}, on the behavior of the density profile.

Problem 1: Let the initial density be defined as in (4.38). In this case initial velocity is scaled by a factor v_{max} and therefore we get $v_\ell = 12m/s$ and $v_r = 8m/s$. Numerical results are plotted in Figure 4.6.

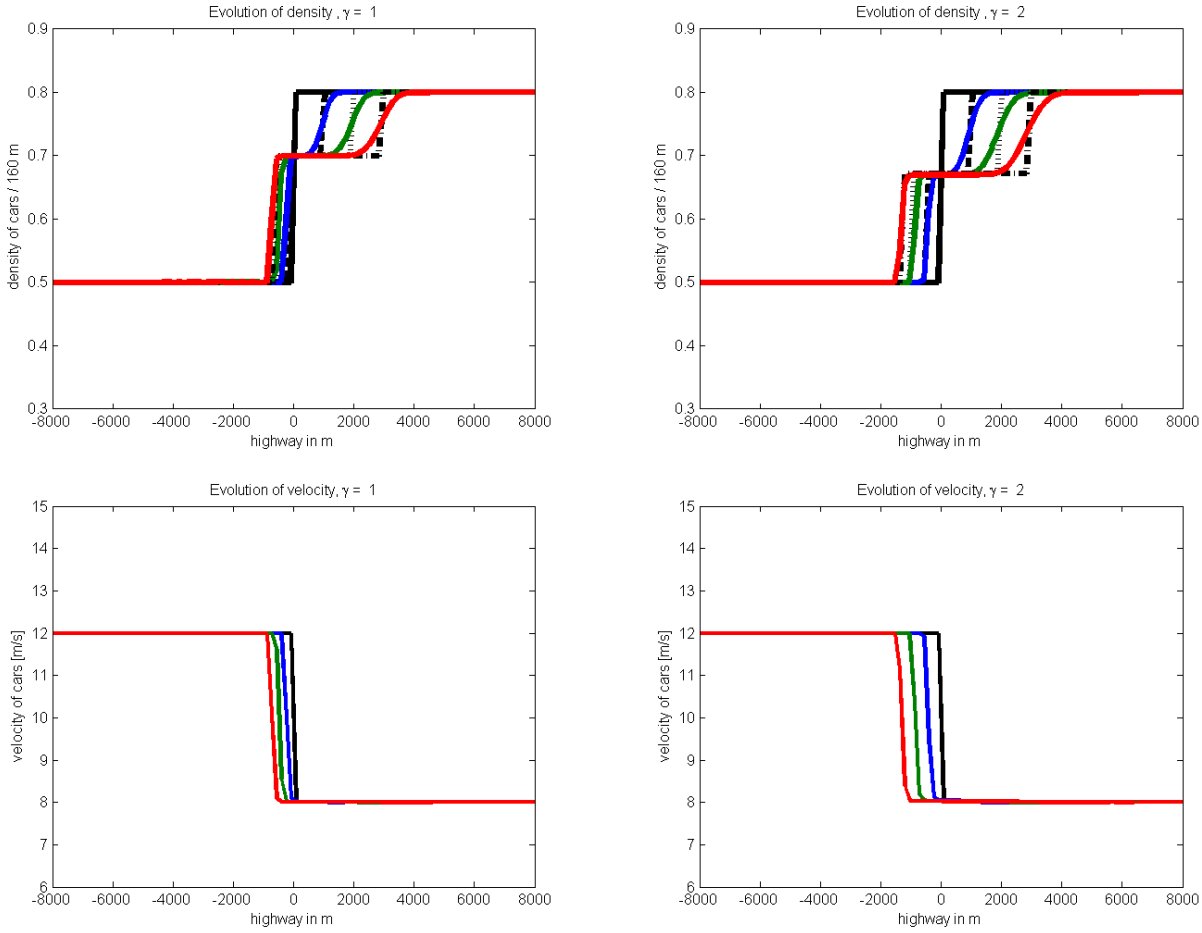

Figure 4.6: *Solution of the Rascle model with Riemann data* $\rho_\ell = 0.8$, $v_\ell = 12\ m/s$, $\rho_r = 0.6$, $v_r = 8\ m/s$. *On the top from left to right are density profiles with* $\gamma = 1$ *and* $\gamma = 2$, *respectively, and their corresponding velocity profiles at the bottom.*

Problem 2: Now take the initial density as in (4.39). Here we have $v_\ell = 12\ m/s$ and $v_r = 20\ m/s$. Numerical results are plotted in Figure 4.7.

Problem 3: Now take the initial density as in (4.40). Here we have $v_\ell = 2\ m/s$ and $v_r = 18\ m/s$. Numerical results are plotted in Figure 4.8.

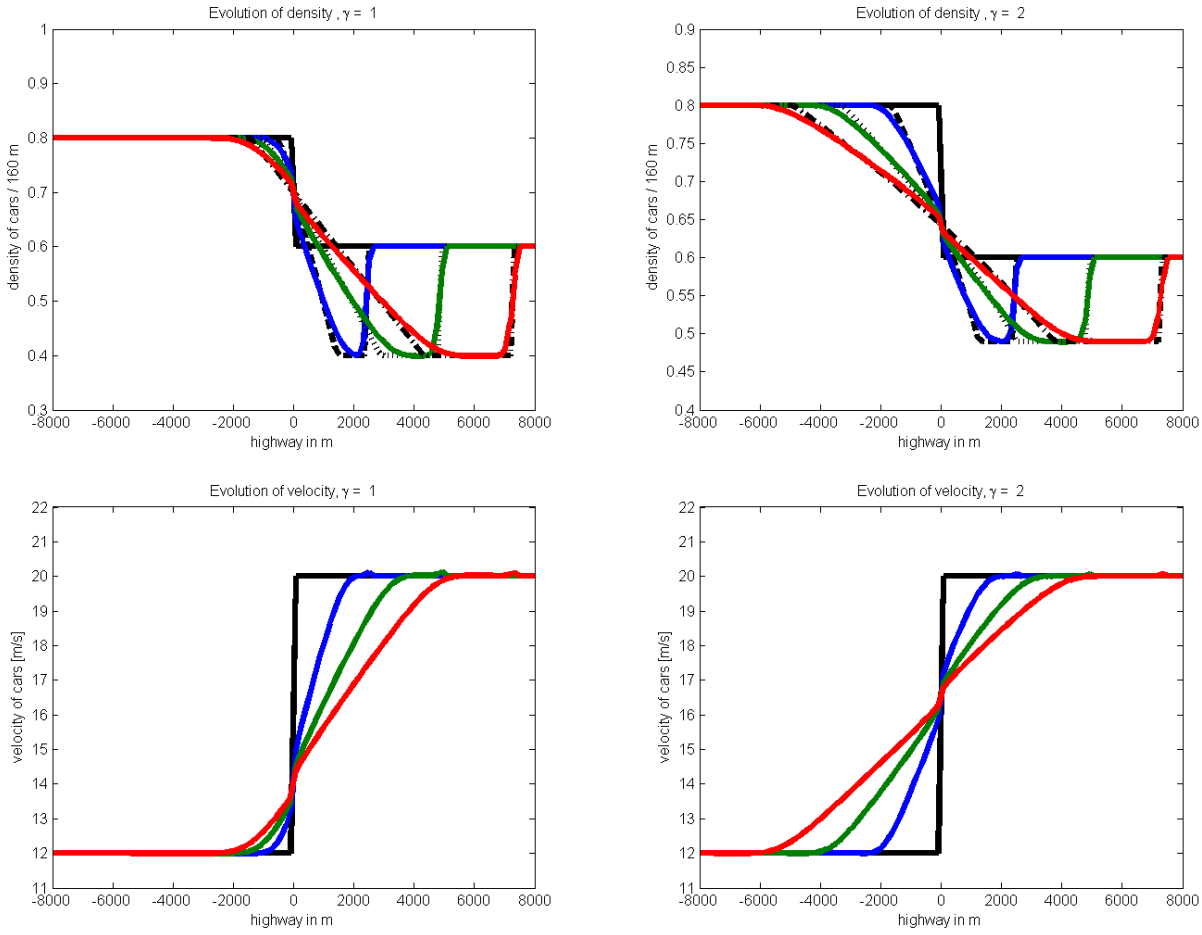

Figure 4.7: *Solution of the Rascle model with Riemann data* $\rho_\ell = 0.8,\ v_\ell = 12\ m/s,\ \rho_r = 0.6,\ v_r = 20\ m/s$. *On the top from left to right are density profiles with* $\gamma = 1$ *and* $\gamma = 2$, *respectively, and their corresponding velocity profiles at the bottom.*

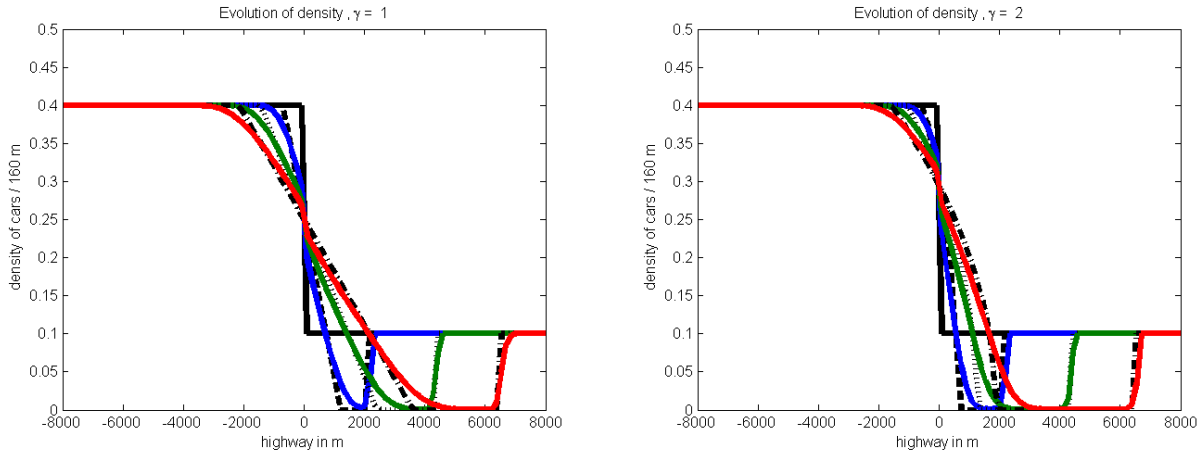

(a) with $\gamma = 1$

(b) with $\gamma = 2$

Figure 4.8: *Density profiles of the Rascle model with Riemann data* $\rho_\ell = 0.4,\ v_\ell = 2\ m/s,\ \rho_r = 0.1,\ v_r = 18\ m/s$.

Problem 4: Now take the initial density as in (4.41), and initial velocity $v_\ell = 12\ m/s$ and $v_r = 20\ m/s$. Numerical results are plotted in Figure 4.9.

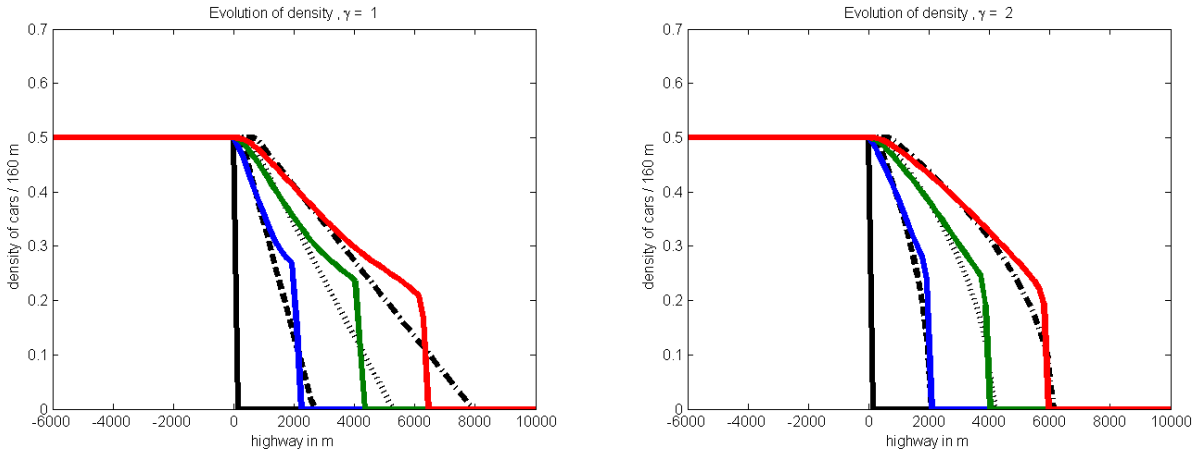

(a) with $\gamma = 1$ (b) with $\gamma = 2$

Figure 4.9: *Density profiles of the Rascle model with Riemann data* $\rho_\ell = 0.5,\ v_\ell = 12\ m/s,\ \rho_r = 0,\ v_r = 20\ m/s$.

Problem 5: Finally consider the initial density as in (4.42) with initial velocity $v_\ell = 10\ m/s$ and $v_r = 10\ m/s$. Numerical results are plotted in Figure 4.9.

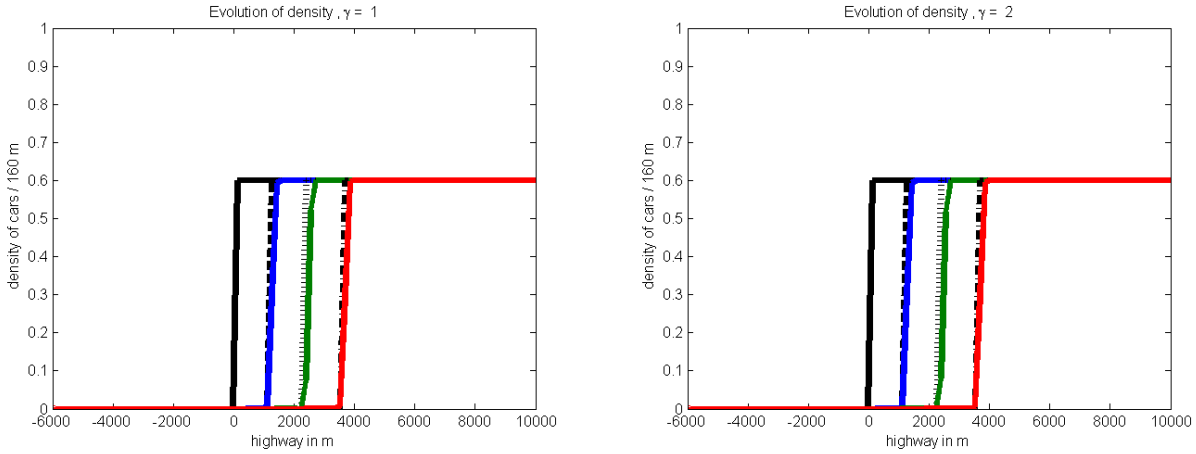

(a) with $\gamma = 1$ (b) with $\gamma = 2$

Figure 4.10: *Density profiles of the Rascle model with Riemann data* $\rho_\ell = 0,\ v_\ell = 10\ m/s,\ \rho_r = 0.5,\ v_r = 10\ m/s$.

4.4 Qualitative Properties of the Aw-Rascle Model

- The Aw-Rascle model defined by the system (4.6) is strictly hyperbolic, except for $\rho = 0$ where the two eigenvalues of the corresponding Jacobian matrix collapse.
- For any pressure function $p(\rho)$ satisfying assumptions (4.3), and any chosen initial state $U_0 = (U_\ell, U_r)$ in the bounded convex region

$$\Omega \;:=\; (\rho, v) | 0 \leq v \leq v_{max} - p(\rho), \;\; \rho \geq 0, \; 0 \leq v \leq v_{max},$$

  there exists a unique solution to the Riemann problem associated with (4.6) and the data U_0.
- The Rascle model (4.6) satisfies all the natural qualitative requirements that one can impose: the velocities and the densities remain nonnegative all times. They stay in a bounded invariant region Ω defined above, and therefore, they remain bounded from above.
- The propagation speed of any wave involving a state U is at most equal to its velocity v, this means, there is no information travelling faster than the velocity of cars.
- The model always predicts the natural waves: shocks when braking, contacts when following, rarefactions, possibly with appearance of vacuum, when accelerating, instabilities near vacuum, especially with a few slow drivers ahead.
- When one of the Riemann data is near the vacuum, the solution presents the instabilities discussed in section 4 of [2].

Chapter 5

Numerical Comparisons of the LWR Model with the Aw-Rascle Model

In this chapter we present numerical comparisons of the LWR model (3.6) with the Aw-Rascle model (4.2), already discussed in the previous chapters, by giving differences and similarities between them. All our results presented in this chapter are computed under the assumption the maximum concentration of cars on the considered highway is unity, i.e., $\rho_{max} = 1$. We study different situations with various choices of parameters in our models such as the maximum velocity v_{max}, as well as γ that appears in the Aw-Rascle model. In all numerical experiments treated in this chapter we propose two different choices of γ : we choose $\gamma = 1$ and $\gamma = 2$. In this chapter the input velocity in the Aw-Rascle model is computed from the following density-velocity relationship

$$v(\rho) \quad = \quad v_{max}(1 - \rho) \tag{5.1}$$

since the maximum density is $\rho_{max} = 1$ in all numerical tests. We assess the comparisons of our models by first considering the simple case where $v_{max} = 1$, and then we extend this case to a realistic one in which the considered highway, density and velocity variables are respectively measured in realistic units: m (meter), $1/m$, and m/s (meter/second). In the plots of this subsection, the black solid line represents the initial state of both models, the blue line is the solution of the Rascle model at $t = 2$, the green line is the solution of the Rascle model at $t = 4$, the red line represents the solution of the Rascle model at $t = 6$, the dashed-line represents the solution of the LWR model at $t = 2$, the dotted-line is the solution of the LWR model at $t = 4$, and finally the solution of the LWR model at $t = 6$ is manifested by the dashed-dotted line.

5.1 Simplified models

We simplify our computations by choosing the maximum velocity $v_{max} = 1$. Here we study the density profiles of the following four distinct Riemann problems of the two models of our interest and present the comparisons between them.

Problem 5.1 We start with a situation in which more cars are concentrated on the right of the discontinuity with initial state

$$\rho(x, 0) \quad = \quad \begin{cases} 0.5, & x < 0, \\ 0.8, & x > 0. \end{cases} \tag{5.2}$$

In this case, the exact solution of the LWR model is a left-going shock wave of the form (3.13), moving at speed $s = -0.3$ computed from (3.14). In order to solve the Aw-Rascle model with the same initial density we first compute the initial velocity from (5.1). Hence the initial velocity for the Aw-Rascle model associated with the initial density (5.2) is given by

$$v(x,0) = \begin{cases} 0.5, & x < 0, \\ 0.2, & x > 0. \end{cases}$$

For the Aw-Rascle model, since $v_r < v_\ell$, the corresponding exact solution is given by a left-going shock wave followed by a contact discontinuity moving at the speed of the leading cars $v_r = 0.2$. This is already described in Case 1 of the later chapter. Numerical results are plotted in Figures 5.1 (evolution of density and velocity).

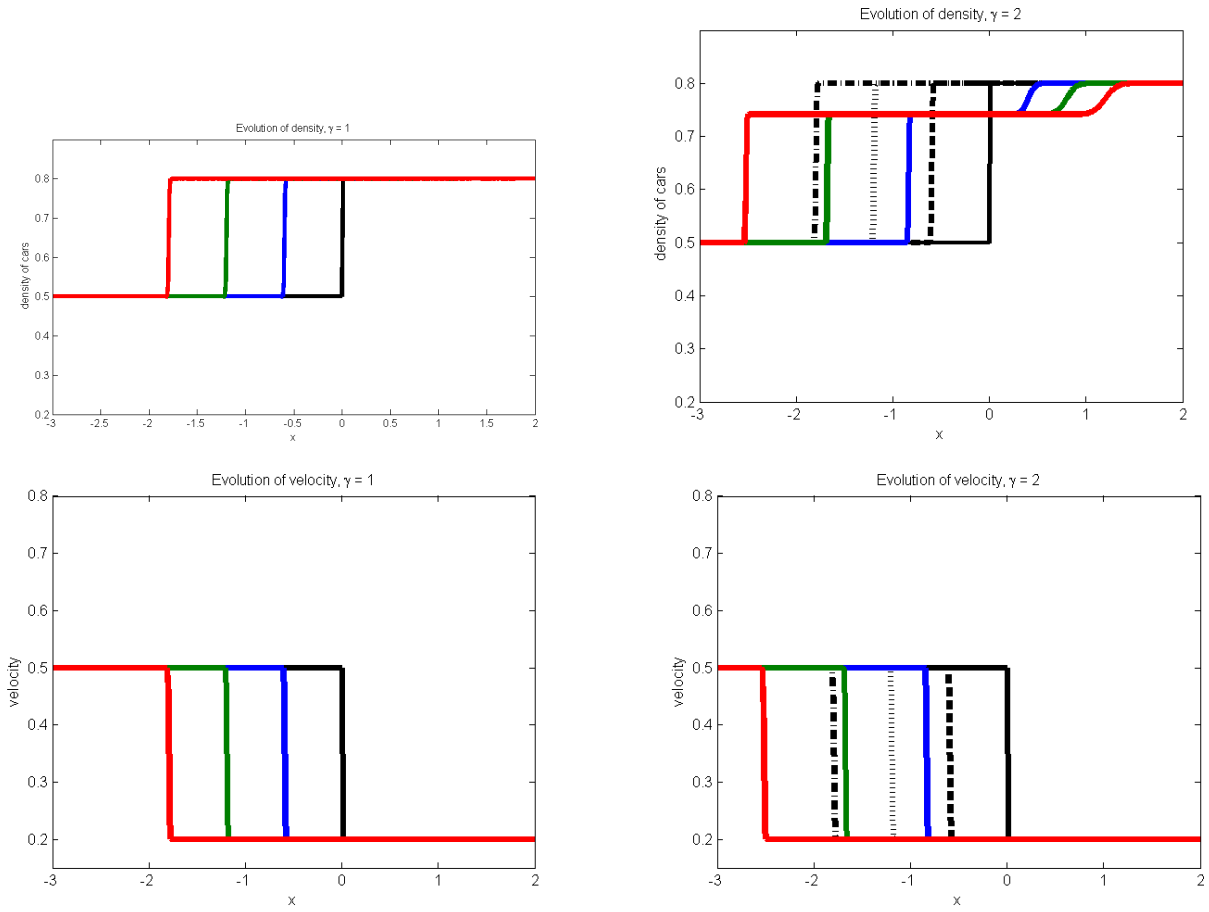

Figure 5.1: *Density profiles of the two models for the Riemann problem with* $\rho_\ell = 0.5$, $v_\ell = 0.5$, $\rho_r = 0.8$, *and* $v_r = 0.2$. *On the top from left to right we have density profiles with* $\gamma = 1$ *and* $\gamma = 2$, *respectively, and their corresponding velocity profiles at the bottom. Here the black solid line represents the initial state of both models, the blue line is the solution of the Rascle model at* $t = 2$, *the green line is the solution of the Rascle model at* $t = 4$, *the red line represents the solution of the Rascle model at* $t = 6$, *the dashed-line represents the solution of the LWR model at* $t = 2$, *the dotted-line is the solution of the LWR model at* $t = 4$, *and finally the solution of the LWR model at* $t = 6$ *is manifested by the dashed-dotted line.*

Fixing $\gamma = 1$ in the Rascle model, the intermediate state ρ_m coincides with the right state ρ_r; this is proven in the last section of this chapter. Hence the wave of the second family in the Rascle model disappears and the solution is only a shock wave propagating to the right at exactly the same speed $s = 0.2$ as that of the shock of the LWR model. Numerical solutions in this Riemann problem are the same in both models and are presented in Figure 5.1. About the numerical aspects, this shock wave is properly captured by the Godunov scheme applied to simulate our models. Now setting $\gamma = 2$, we have $\rho_m \neq \rho_r$. Thus we have an additional second wave (contact discontinuity) of the Rascle model going to the right. We observe from 5.1 that the wave of the Rascle model is faster than the wave of the LWR model, this is because some cars of the Rascle model are distributed in the intermediate state ρ_m, while cars of the LWR are dense in a certain range of the chosen highway: cars of the Rascle model are more distributed than cars of the LWR model. In our tests, but not presented in this thesis, we observe that the contact discontinuity of the second family is properly resolved as we refine the mesh.

Problem 5.2 Now let us consider the initial state

$$\rho(x,0) = \begin{cases} 0.8, & x < 0, \\ 0.6, & x > 0. \end{cases}$$

With this data the corresponding initial velocity, computed as above, is given by

$$v(x,0) = \begin{cases} 0.2, & x < 0, \\ 0.4, & x > 0. \end{cases}$$

For the LWR model the exact solution of this problem is a left-going rarefaction wave, since $\rho_\ell > \rho_r$. As for the Aw-Rascle model, the exact solution is a rarefaction wave followed by a contact discontinuity. This last wave disappears for $\gamma = 1$, since in this particular case $\rho_m = \rho_r$. Hence we have for both models a single left-going rarefaction wave moving at the same speed, but we observe the difference when $\gamma = 2$. With this choice the rarefaction wave of the Rascle model moves faster than the wave of the LWR model as shown in Figure 5.2.

Problem 5.3 Now set the initial state

$$\rho(x,0) = \begin{cases} 0.4, & x < 0, \\ 0.1, & x > 0, \end{cases}$$

with initial velocity

$$v(x,0) = \begin{cases} 0.6, & x < 0, \\ 0.9, & x > 0. \end{cases}$$

The exact solution of the LWR model is a right-going rarefaction wave since $\rho_\ell > \rho_r$. For the Rascle model the solution is a rarefaction wave moving to the right connected to a vacuum state followed by a fast contact discontinuity going to the right with speed $v_r = 0.9$. The results are shown in Figure 5.3.

We have with $\gamma = 1$, the solution is a right-going rarefaction wave for both models, while with $\gamma = 2$ the solution of the Rascle model presents an artificial jump that cannot be captured by the numerical scheme we used, even if we refine the mesh it cannot be reduced. In this case the LWR model present nice results without any jump.

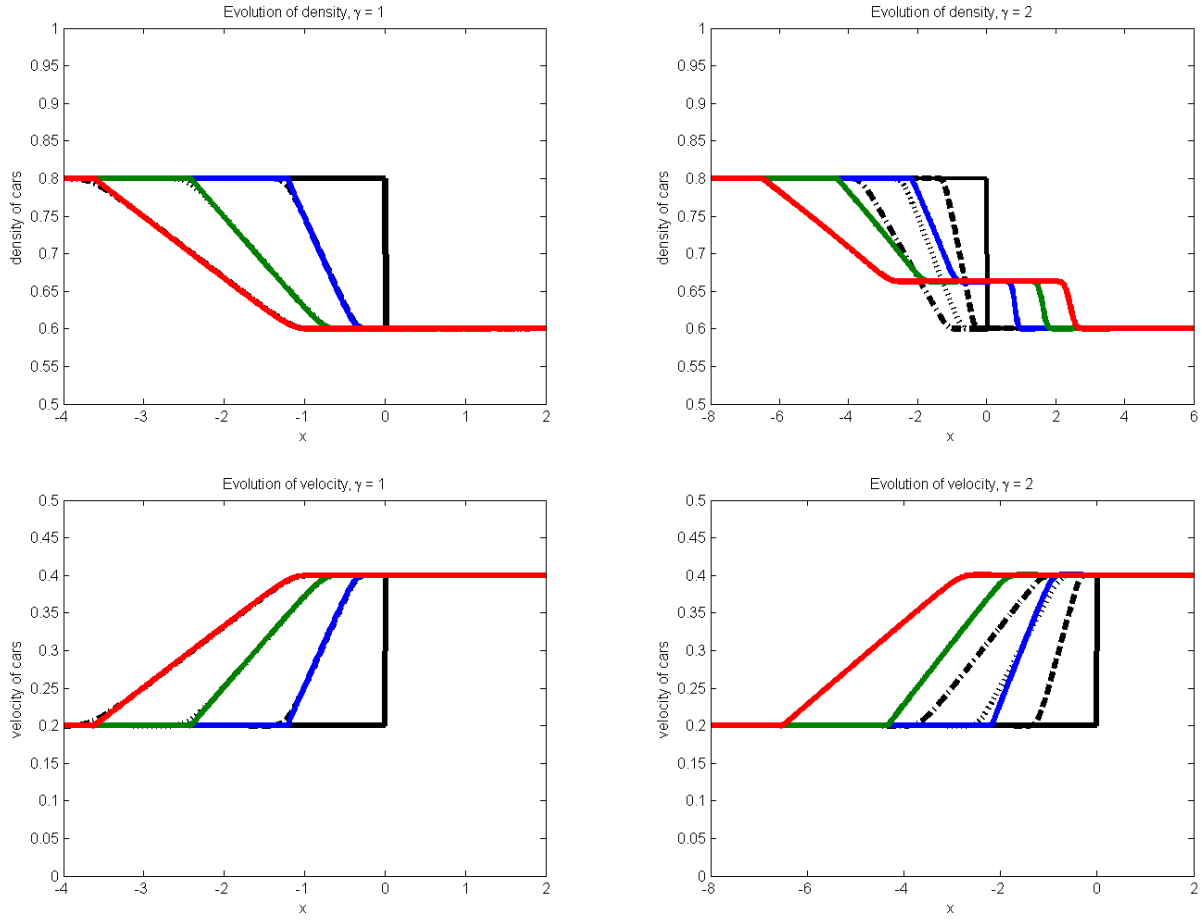

Figure 5.2: *Solution of the Rascle model with Riemann data* $\rho_\ell = 0.8,\ v_\ell = 0.2,\ \rho_r = 0.6,$ *and* $v_r = 0.4$. *On the top from left to right we have density profiles with* $\gamma = 1$ *and* $\gamma = 2,$ *respectively, and their corresponding velocity profiles at the bottom. The black solid line represents the initial state of both models, the blue line is the solution of the Rascle model at* $t = 2$, *the green line is the solution of the Rascle model at* $t = 4$, *and the red line represents the solution of the Rascle model at* $t = 6$.

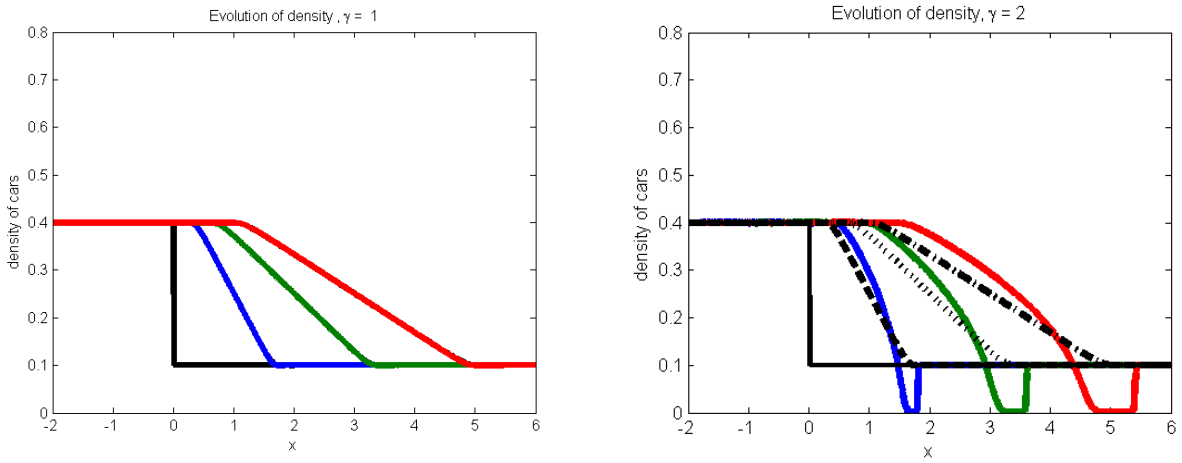

(a) with $\gamma = 1$ (b) with $\gamma = 2$

Figure 5.3: *Density profiles of the two models with Riemann data* $\rho_\ell = 0.4$, $v_\ell = 0.6$, $\rho_r = 0.1$, *and* $v_r = 0.9$. *The black solid line represents the initial state of both models, the blue line is the density of the Rascle model at* $t = 2$, *the green line is the density of the Rascle model at* $t = 4$, *and the red line represents the density of the Rascle model at* $t = 6$.

Problem 5.4 Consider the following Riemann data

$$\rho(x,0) = \begin{cases} 0.5, & x < 0, \\ 0, & x > 0, \end{cases}$$

with initial velocity

$$v(x,0) = \begin{cases} 0.5, & x < 0, \\ 1, & x > 0. \end{cases}$$

For both choices of γ, we have a single rarefaction wave for the two models as shown in Figure 5.4.

Problem 5.5 Finally we study a group of moving cars followed by an empty road with initial state

$$\rho(x,0) = \begin{cases} 0, & x < 0, \\ 0.5, & x > 0, \end{cases}$$

with initial velocity

$$v(x,0) = \begin{cases} 1, & x < 0, \\ 0.5, & x > 0. \end{cases}$$

In this case we have a right-going shock wave for the LWR model, and a single contact discontinuity for the Aw-Rascle model as shown in Figure 5.5. Here we see that the shock wave of the LWR model coincides with the contact discontinuity of the Rascle model, because this shock moves exactly at the same speed as the contact discontinuity: $s = 0.5 = v_r$.

- For $\gamma = 1$ the solutions of LWR model are the same as for the Aw-Rascle model.
- To be able to see the significant effects of the second-order model, i.e., the Aw-Rascle model, we should increase the value of γ.

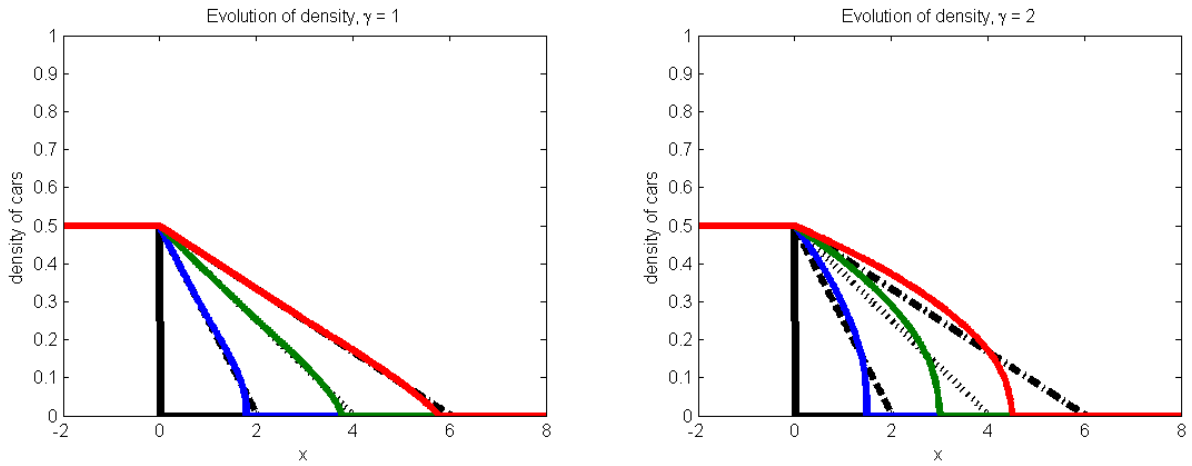

(a) with $\gamma = 1$ (b) with $\gamma = 2$

Figure 5.4: *Density profiles of the two models with Riemann data* $\rho_\ell = 0,\ v_\ell = 1,\ \rho_r = 0.5,$ *and* $v_r = 0.5$. *The black solid line represents the initial state of both models, the blue line is the density of the Rascle model at* $t = 2$, *the green line is the density of the Rascle model at* $t = 4$, *and the red line represents the density of the Rascle model at* $t = 6$.

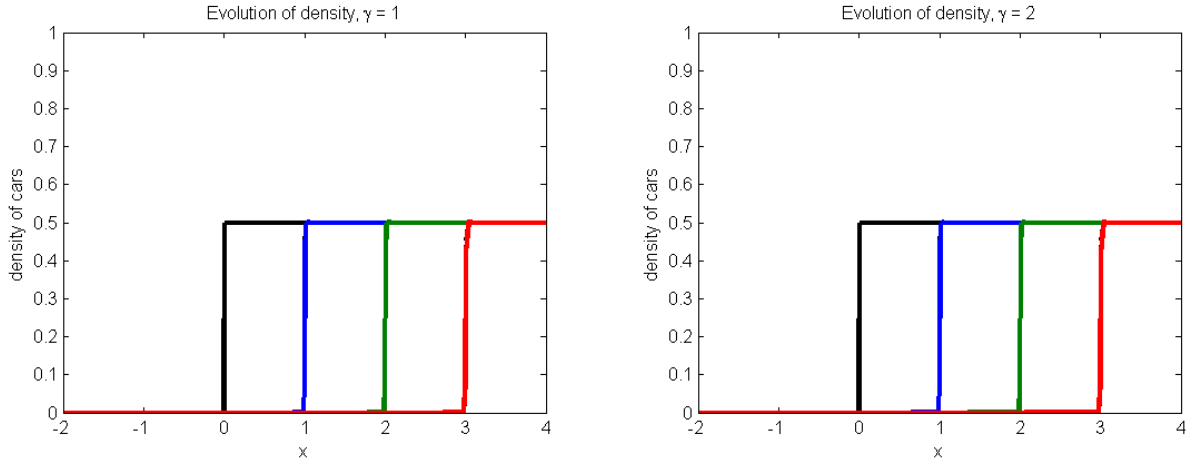

(a) with $\gamma = 1$ (b) with $\gamma = 2$

Figure 5.5: *Density profiles of the two models with Riemann data* $\rho_\ell = 0,\ v_\ell = 1,\ \rho_r = 0.5,$ *and* $v_r = 0.5$. *The black solid line represents the initial state of both models, the blue line is the density of the Rascle model at* $t = 2$, *the green line is the density of the Rascle model at* $t = 4$, *and the red line represents the density of the Rascle model at* $t = 6$.

5.2 Realistic Problem

Now we extend the above results for the simple case by choosing, instead of assuming v_{max} to be unit, realistic data. Here we perform a numerical experiment for 6 minutes for a highway of 8 km in spatial grig points with step size $\Delta x = 80$ meters. We want to simulate the traffic flow for 6 minutes with some fixed parameter v_{max} measured in $[m/s]$ (meter/second). Like in the late section, initial velocities of the Rascle model are again computed from the density-velocity relationship (5.1). Variables in our models are now scaled by the chosen value of the parameter v_{max}. To be precise we propose $v_{max} = 20\ m/s$.

Problem 1: with initial density (5.2), we present the corresponding results in Figure 5.6.

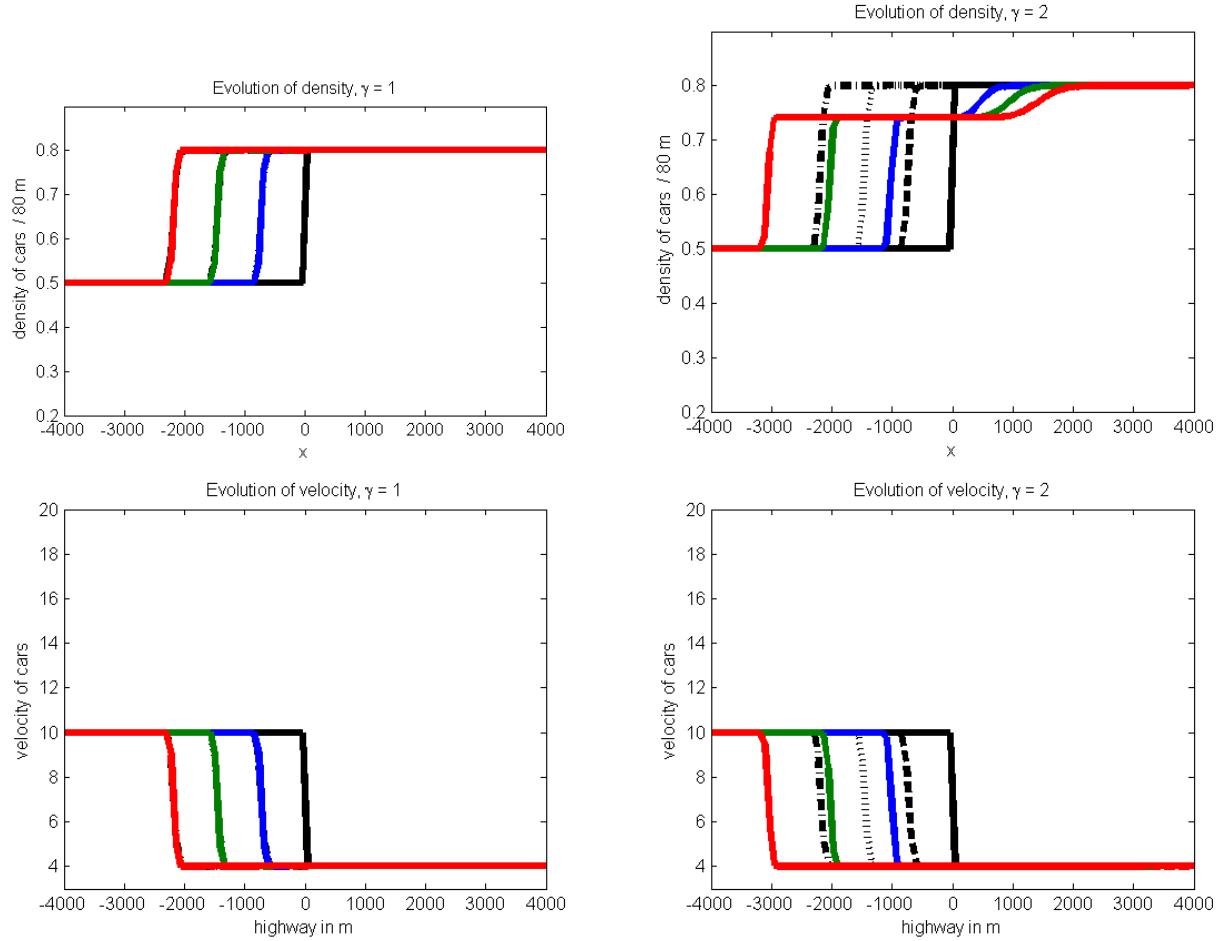

Figure 5.6: *Density profiles of the two models for the Riemann problem with* $\rho_\ell = 0.5$, $v_\ell = 20$, $\rho_r = 0.8$, *and* $v_r = 8$. *Here the black solid line represents the initial state of the two models, the blue solid line is the density of the Rascle model at* 2 *minutes, the green solid line is the density of the Rascle model at* 4 *minutes, the red solid line represents the density of the Rascle model at* 6 *minutes, the dashed-line represents the density of the LWR model at* 2 *minutes, the dotted-line is the density of the LWR model at* 4 *minutes, and finally the density of the LWR model at* 6 *minutes is manifested by the dashed-dotted line.*

From these results we observe the difference between the two models only when $\gamma = 2$. Initially the shock wave of both models is located at distance $x = 0$ m. After two minutes we see from Figure 5.6 that the shock of the LWR model is located at distance of $x = -849$ m while the shock of the Rascle model is already at $x = -1091$ m, i.e., at 242 m ahead. As time advances the gap between them grows up; after minutes the Rascle shock is at 889 m ahead of the LWR shock. In order words drivers of the Rascle model are faster than drivers of the LWR model all the time. This can be explained by the fact that part of the resultant wave (contact discontinuity) of the Rascle model moves to the right with a big speed v_r, and other part (shock) goes to the left with a speed bigger than that of the LWR shock. Hence on the left side of the discontinuity we have less concentration of cars of the Rascle model, here the density for this model lies in the interval $[0.5, 0.74]$, while the density for the LWR model varies in the interval $[0.5, 0.8]$. Therefore drivers of the LWR model present a faster braking.

Problem 2: with initial density (5.2), we present the corresponding results in Figure 5.7.

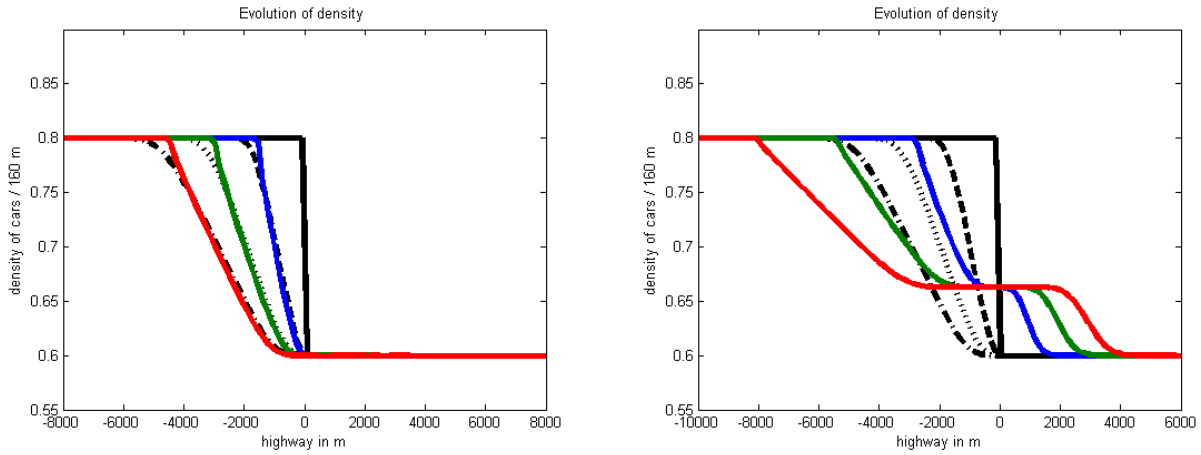

(a) with $\gamma = 1$ (b) with $\gamma = 2$

Figure 5.7: *Density profiles of the two models for the Riemann problem with* $\rho_\ell = 0.8$, $v_\ell = 4$, $\rho_r = 0.6$, *and* $v_r = 8$. *Here the black solid line represents the initial state of the two models, the blue solid line is the density of the Rascle model at* 2 *minutes, the green solid line is the density of the Rascle model at* 4 *minutes, the red solid line represents the density of the Rascle model at* 6 *minutes, the dashed-line represents the density of the LWR model at* 2 *minutes, the dotted-line is the density of the LWR model at* 4 *minutes, and finally the density of the LWR model at* 6 *minutes is manifested by the dashed-dotted line.*

Problem 3: with initial density (5.3), we present the corresponding results in Figure 5.8.

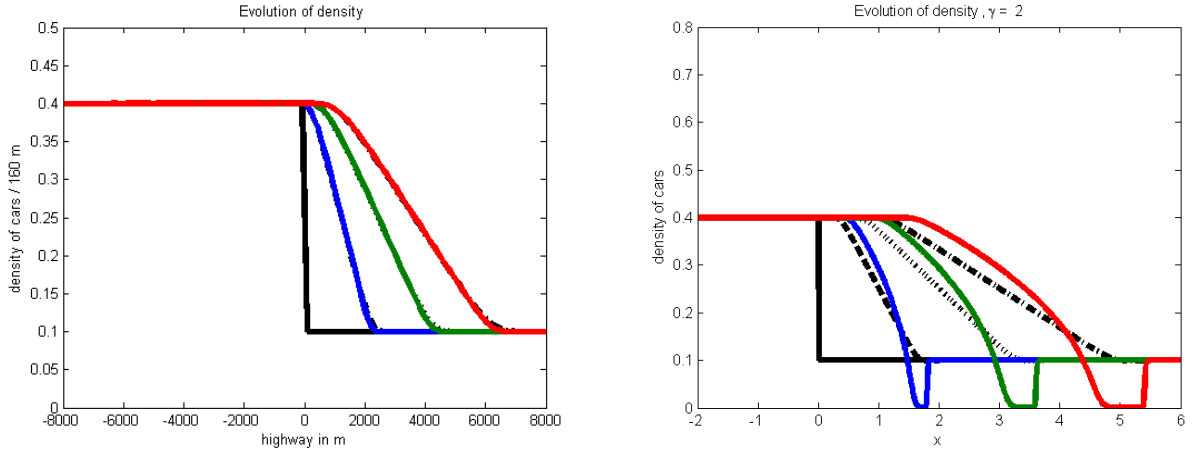

(a) with $\gamma = 1$ (b) with $\gamma = 2$

Figure 5.8: *Density profiles of the two models for the Riemann problem with* $\rho_\ell = 0.4$, $v_\ell = 12$, $\rho_r = 0.1$, *and* $v_r = 18$. *Here the black solid line represents the initial state of the two models, the blue solid line is the density of the Rascle model at* 2 *minutes, the green solid line is the density of the Rascle model at* 4 *minutes, the red solid line represents the density of the Rascle model at* 6 *minutes, the dashed-line represents the density of the LWR model at* 2 *minutes, the dotted-line is the density of the LWR model at* 4 *minutes, and finally the density of the LWR model at* 6 *minutes is manifested by the dashed-dotted line.*

Problem 4: with initial density (5.4), we present the corresponding results in Figure 5.9.

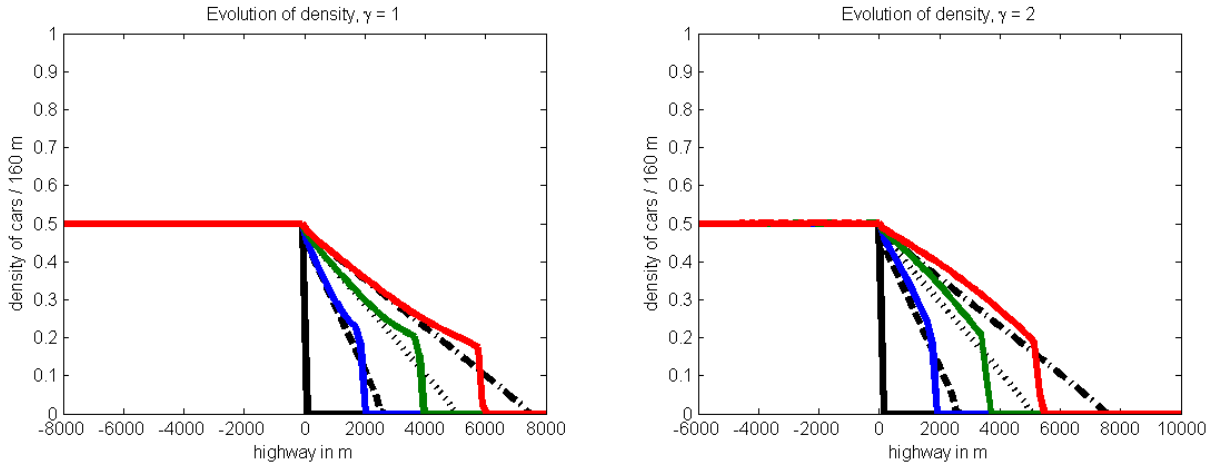

(a) with $\gamma = 1$ (b) with $\gamma = 2$

Figure 5.9: *Density profiles of the two models for the Riemann problem with* $\rho_\ell = 0.5$, $v_\ell = 10$, $\rho_r = 0$, *and* $v_r = 20$. *Here the black solid line represents the initial state of the two models, the blue solid line is the density of the Rascle model at* 2 *minutes, the green solid line is the density of the Rascle model at* 4 *minutes, the red solid line represents the density of the Rascle model at* 6 *minutes, the dashed-line represents the density of the LWR model at* 2 *minutes, the dotted-line is the density of the LWR model at* 4 *minutes, and finally the density of the LWR model at* 6 *minutes is manifested by the dashed-dotted line.*

Problem 5: with initial density (5.5), we present the corresponding results in Figure 5.10.

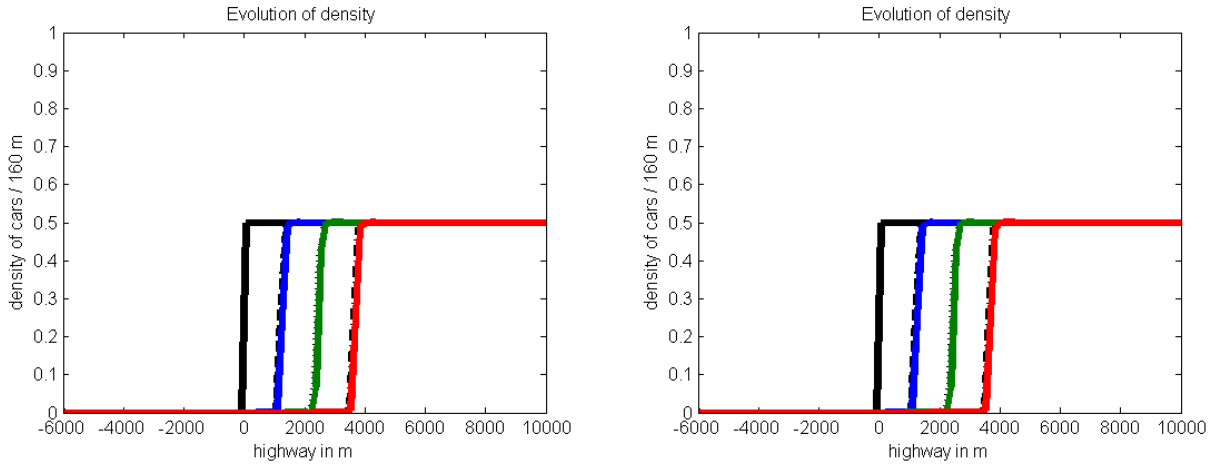

(a) with $\gamma = 1$ (b) with $\gamma = 2$

Figure 5.10: *Density profiles of the two models for the Riemann problem with* $\rho_\ell = 0$, $v_\ell = 20$, $\rho_r = 0.5$, *and* $v_r = 10$. *Here the black solid line represents the initial state of the two models, the blue solid line is the density of the Rascle model at* 2 *minutes, the green solid line is the density of the Rascle model at* 4 *minutes, the red solid line represents the density of the Rascle model at* 6 *minutes, the dashed-line represents the density of the LWR model at* 2 *minutes, the dotted-line is the density of the LWR model at* 4 *minutes, and finally the density of the LWR model at* 6 *minutes is manifested by the dashed-dotted line.*

5.3 Observations and some Remarks

We end this chapter with the following observations from our numerical tests discussed in the two later subsections above.

- with $\gamma = 1$, cars of the LWR model are moving at almost the same speed as those of the Rascle model. This is because, in the Rascle model, the intermediate state ρ_m is simply

$$\begin{aligned} \rho_m &= v_\ell - v_r + \rho_\ell, \\ &= \rho_r \end{aligned}$$

by the use of (5.1). Hence in this case the speed of the Rascle shock wave (4.27) is reduced to

$$\begin{aligned} s &= \frac{\rho_r v_r - \rho_\ell v_\ell}{\rho_r - \rho_\ell}, \\ &= v_{max}\Big(1 - (\rho_r + \rho_\ell)\Big) \end{aligned}$$

after substituting (5.1). This speed is exactly the same as the speed of the shock (3.14) obtained in the LWR model. In the case of rarefaction waves, we also have the wave speeds

$$\lambda(U) = v_{max}(1 - 2\rho)$$

in the LWR model, and the speed of the Rascle rarefaction wave is given by

$$\begin{aligned} \lambda_1(U) &= v - \gamma\rho^\gamma, \\ &= v - \rho \end{aligned}$$

since $\gamma = 1$. Using (5.1) yields

$$\lambda_1(U) = v_{max}(1 - \rho) - \rho.$$

Therefore for a given choice of initial density and fixed maximum velocity $v_{max} = 1$, the rarefaction wave of the LWR model moves exactly at the same speed as the one of the Rascle model. This explains the similarities of the LWR and Aw-Rascle models for the choice of $\gamma = 1$.

- Now increasing the value of γ and setting $\gamma = 2$, the intermediate state of the Rascle model is no longer the same as the right state, which results in the change of the wave speeds in both shock and rarefaction wave cases. With this choice of the parameter γ, we observe that
  - the shock wave of the Rascle model is faster than the shock of the LWR model as shown in the Figures 5.1 - 5.5. This means that drivers of the LWR model show a faster breaking than those of the Aw-Rascle model.
  - We observe a fast rarefaction wave in the Aw-Rascle model, which means drivers of the LWR model accelerate faster than drivers of the Rascle model.

Chapter 6

Conclusion

In this thesis, we have considered two macroscopic traffic flow models: the LWR and Aw-Rascle models. The LWR model, which is a quasi-linear first order partial differential equation, has been used to predict the density and velocity profiles at certain points of a highway of 16 km after 6 minutes, and the Aw-Rascle model was considered in order to incorporate second-order effects. The Aw-Rascle model incorporates the idea that drivers only care about what is happening in front of them not in behind. We have solved the Riemann problems associated with these two models and arbitrary chosen initial data. We treated different Riemann problems analytically and then applied the first order Godunov-type approximation for their numerical simulations. Regarding the numerical comparisons of the LWR and Aw-Rascle models we presented in the later chapter above, we observed, while simulating associated Riemann problems, that drivers of the LWR model present a faster braking and accelerating comparing to those of the Aw-Rascle model. This is explained by the fact that cars of the LWR model are densely distributed than cars of the Rascle model.

Depending on the choices of the parameter γ in the Aw-Rascle model we have seen that the Aw-Rascle model is equivalent to the LWR model when we set $\gamma = 1$, that is, when the pressure function is a linear function of the density ρ, whereas for $\gamma = 2$, i.e., with high pressure, in the order of power of density, drivers of the Rascle model tend to be faster than those of the LWR model due to an additional intermediate state that is not existed in the LWR model. This intermediate state explains the reason why cars in the Aw-Rascle model are less densely distributed comparing to cars in the LRW model.

We have verified the qualitative behaviour of different flow variables in our models and the outcome of different parameters of the model has also been presented. While studying the Rascle model all the inconsistencies of second-order models presented by Daganzo and other authors have been disappeared. The Aw-Rascle model predicts instabilities near the vacuum, when very light traffic flow is concerned. With this consistency we have ascertained that it provides an efficient way and easy-to-use method for modelling traffic flows of our interest. For instance, it can be extended to model traffic problems on road networks.

Acknowledgements

To God be the Glory!

I express my sincere gratitude to my supervisor prof. dr. Axel Klar, as well as my assistant supervisor dr. Raul Borsche, who always provided positive encouragement, guidance, valuable discussions, meaningful suggestions during my thesis writing. prof. dr. Axel Klar, your ability and constructive direction made all this possible. To dr. Raul Borsche, I would not have made any headway but for your availability despite my relentless prodding. Thank you both for affording me the opportunity to work with you.

I would like to express my sincere gratitude to dr.ir. J.H.M. ten Thije Boonkkamp for his kindness, initiative and interest in reading this project. My thanks go to all the lecturers and staff of the Departments of Mathematics of Technical University of Eindhoven, Holland and Technical University of Kaiserslautern, Germany. My wholehearted thanks to all the brains behind the Erasmus Mundus Scholarship Program who gave me the opportunity to be in this Masters program. This masters degree has been fully and generously supported by the European Union Erasmus Mundus Scholarship Program in Industrial Mathematics.

I am indebted to dr. Oliver Tse, mr. Florien Nsanganwimana, mr. Vidit Maheshwari, and mr. Luc Muhirwa for their open discussions, guidance and encouragement at every stage of my studies. Without their company I would'not have been memorable. I say God bless them for their help.

I am indebted to my lovely parents, sisters and brother for being there for me. I appreciate your love, moral, understanding, patience and support during the up and down periods, you constantly remind me the value of a good education, and encourage me to make the most of my education, your encouragement has kept me going up to this point. I am sending my grateful appreciation to all my classmates, AERK family and friends for the wonderful atmosphere we shared during my stay in Europe, your help and support during my studies, I say my God bless all of us.

Bibliography

[1] R. M. M. Mattheij, S. W. Rienstra, and J. H. M. ten Thije Boonkkamp, *Partial Differential Equations, Modeling, Analysis, Computation*, 2005.

[2] A. Aw and M. Rascle, *Resurrection of Second Order Models of Traffic Flow*, SIAM Journal on Applied Mathematics, 2010.

[3] Thoe, Dale W. and E.C. Zachmanoglou. *Introduction to Partial Differential Equations with Applications*. Dover Publications, Inc., New York: 1986, p. 76-86.

[4] Germund Dahlquist, Ake Björck, *Numerical Methods in Scientific Computing*, Society for Industrial and Applied Mathematics, Volume 1, 2008.

[5] DYKwak, *Numerical Partial Differential Equations*, Lecture Notes, 2007.

[6] Yadong Lu, S.C. Wong, Mengping Zhang, Chi-Wang Shu, *The entropy solutions for the Lighthill-Whitham-Richards traffic flow model with a discontinuous flow-density relationship*, Notes, 2000.

[7] G.B. WHITHAM, *Linear and nonlinear waves*, John Wiley and Sons, New York, 1974.

[8] Peter D. Lax, *Hyberbolic Systems of Conservation Laws and the Mathematical Theory of Shock Waves*, SIAM, Philadelphia, 1973.

[9] Randall J. LeVeque, *Numerical Methods for Conservation Laws*, University of Washington, 1990.

[10] E. F. Toro, *Riemann Solvers and Numerical Methods for Fluid Dynamics*, 1999.

[11] A. Klar and R. Wegener, *Kinetic derivation of macroscopic anticipation models for vehicular traffic*, SIAM J. Appl. Math. 60, p. 1749-1766, (2000).

[12] Axel Klar, Reinhart D. Khne and Raimund Wegener, *Mathematical Models for Vehicular Traffic*, 2000.

[13] Benedetto Piccoli and Andrea Tosin, *Vehicular Traffic: A Review of Continuum Mathematical Models.* Springer, 2009, p. 9727-9749.

[14] N. BELLOMO and M. DELITALA, *On the Mathematical Theory of Vehicular Traffic Flow I. Fluid Dynamic and Kinetic Modeling*, 2002.

[15] Christopher Lustri, *Continuum Modelling of Traffic Flow*, 2010.

[16] C. Daganzo. *Requiem for Second-order Fluid Approximation to Traffic Flow.* Transport Res. B 29 (1995), p. 277-286

[17] Yadong Lu, S.C. Wong, Mengping Zhang, Chi-Wang Shu and Wenqin Chen, *Explicit Construction of Entropy Solutions for the Lighthill-Whitham-Richards Traffic Flow Model with a Non-smooth Flow-density Relationship*, Brown University,Division of Applied Mathematics, 2006.

[18] M. J. Lighthill and G. B. Whitham, *On Kinematic Waves II. A Theory of Traffic Flow on Long Crowded Roads*. The Royal Society of London. Series A, Mathematical and Physical Sciences, Vol. 229, 1955.

[19] Douglas A. Kurtze and Daniel C. Hong, *Traffic Jams, Granular Flow, and Soliton Selection*. Phys. Rev. E, Vol. 52, p. 218-221.

[20] M. Rascle, *An Improved Macroscopic Model of Traffic Flow: Derivation and Links with the Lighthill-Whitham Model*, Laboratoire de MathCmatiques, Univ. de Nice, 2002.

[21] P. D. Lax, *Hyperbolic Systems of Conservation Laws and the Mathematical Theory of Shock Waves*. CBMF-NSF Regional Series In Applied Math., SIAM Philadelphia, 1973.

[22] H. Greenberg. "*An Analysis of Traffic Flow*. Operationa Research, 7 (1959) 7885.

[23] R. T. Underwood. "*Speed, Volume, and Density Relationships: Quality and theory of traffic flow*. Yale Bureau of Highway Traffic, 1961, 141188.

[24] P. I. Richards."*Shockwaves on the Highway*. Operational Research, 4 (1956) 4251.

[25] Gould, Harvey and Jan Tobochnik. *Numerical Simulation of Macroscopic Traffic Equations*. Computing in Science and Engineering, September/October 1999, p. 89-99.

[26] D. Serre, *Systems of Conservation Laws*, Diderot, Paris, France, 1996.

[27] Oleinik 0. *Discontinuous Solutions of Nonlinear Differential Equations*. Usp. Math. Nuuk. (N.S.) 12, (3-73), 1957.

[28] Newell G. F. *Nonlinear Effects in the Dynamics of Car-following*. Oper. Res. 209-229, 1961.

[29] RAINER ANSORG, *What Does the Entopy Condition Mean in Traffic Flow Theory*. Oper. Res. p. 133-143, 1990.

[30] Godlewski, E., P.A. Raviart. *Hyperbolic Systems of Conservation Laws*. Ellipses, Paris, 1991.

[31] Kružkov, S. N. *First Order Quasilinear Equations with Several Independent Variables*. Mat. Sb. (N.S.) 81 (123) p. 228255, 1970.

[32] Lax, P. D. *Hyperbolic Systems of Conservation Laws and the Mathematical Theory of Shock Waves*. Society for Industrial and Applied Mathematics, Philadelphia, Pa. Conference Board of the Mathematical Sciences Regional Conference Series in Applied Mathematics, 1973.

[33] Transportation Research Board Special Report 165. *Traffic Flow Theory*. Originally published 1975, addendum 1992.

[34] Prof. Dr. Axel Klar, *Numerical Methods for PDEs II*, Lecture Notes, TU Kaiserslautern, 2011/2012.

[35] J. H. M. ten Thije Boonkkamp, *Scientific Computing in Partial Differential Equations*, Lecture Notes, TU/e, 2009-2010.

[36] Mobach, *Numerical Programming* I,II, Lecture Notes, TU/e, 2009-2010.

Declaration

I, the undersigned, hereby declare that this thesis is my original work, and that any work done by others or by myself previously has been acknowledged and referenced accordingly.

.....

Colette Niyitegeka

July, 2012, Kaiserslautern, Germany